

# A Tutorial on Bayesian Analysis of Linear Shock Compression Data

Jason Bernstein\*, Philip C. Myint<sup>1</sup>, Beth A. Lindquist<sup>2</sup>, Justin Lee Brown<sup>3</sup>

<sup>1</sup>Lawrence Livermore National Laboratory, Livermore, CA 94550

<sup>2</sup>Los Alamos National Laboratory, Los Alamos, NM 87545

<sup>3</sup>Sandia National Laboratories, Albuquerque, NM 87123

## Abstract

Gas gun and other shock compression experiments often produce shock wave velocity measurements that are linearly associated with particle velocity. Traditionally, this empirical relationship is quantified with a single Hugoniot curve that is estimated using least squares regression. However, for downstream modeling and simulation tasks, it is often more useful to have multiple Hugoniot curves in the pressure-volume plane that are consistent with the data. We employ Bayesian uncertainty quantification methods as a framework for propagating measurement uncertainty through to model parameters and predictions. Specifically, this tutorial shows how to sample multiple Hugoniot curves in the pressure-volume plane that are consistent with the shock wave-particle velocity measurements in a two-step Bayesian approach. First, we obtain an analytical expression for the posterior distribution of the linear model parameters using Bayesian linear regression. Second, we propagate samples from the posterior distribution through the Rankine-Hugoniot equations to yield Hugoniot curves in the pressure-volume plane. The procedure is demonstrated with publicly available data on argon, copper, and nickel, and compared against bootstrapping and linear regression. The Bayesian procedure is shown to be interpretable, computationally inexpensive, and less sensitive than an alternative bootstrapping approach to the removal of the point in the copper dataset that has the largest particle velocity. As a tutorial on Bayesian methodology for the shock compression community, we provide several derivations and explanations that make this paper self-contained, and made all code and data available at [github.com/llnl/BALSCD](https://github.com/llnl/BALSCD).

## 1 Introduction

Shock compression experiments produce pairs of shock wave-particle velocity measurements at different impact velocities. This data is valuable because it constrains the equation of state (EOS) of materials at extreme pressures and other conditions. For many materials, the relationship between the shock wave and particle velocities appears to be linear, as [Marsh \(1980\)](#) demonstrates for many datasets. An empirically motivated linear model is therefore typically fit to relate the shock wave velocity measurements to the particle velocity measurements. The goal of this tutorial is to show how to quantify uncertainty in the linear model parameters in order to produce Hugoniot curves in the shock wave-particle velocity plane that are consistent with the data. These Hugoniot curves are then propagated through the Rankine-Hugoniot equations in order to obtain Hugoniot curves in the pressure-volume plane, which can assist in fitting parameters in EOS models, such as the Mie-Grüneisen, Debye, Cell, and Cowan models ([More et al., 1988](#); [Wu et al., 2021](#); [Myint et al., 2023](#)). Tables generated from these EOS models can be used in hydrocode simulations ([Robinson et al., 2013](#)), and Hugoniot curves are also important for impedance matching ([Forbes, 2012](#), Ch. 3). The challenges are, therefore, to accurately quantify the uncertainty in the linear model relating shock wave to particle velocity and to efficiently sample Hugoniot curves in the pressure-volume plane that are consistent with this uncertainty.

---

\*Corresponding author: [bernstein8@llnl.gov](mailto:bernstein8@llnl.gov)

There is a growing body of literature on uncertainty quantification of EOS models. In the Bayesian paradigm, uncertainty is characterized by the so-called posterior distribution, which is obtained by combining a prior distribution over the quantities of interest with the experimental measurements using Bayes' rule. Samples from the posterior distribution are useful for propagating uncertainty through forward models to quantities of interest. A commonly-used algorithm for drawing samples of parameters of interest from their posterior distribution is called Markov Chain Monte Carlo (MCMC). This approach is mainly used when the posterior distribution cannot be sampled directly. This situation arises, for example, when there are many parameters that require calibration and these parameters are non-linearly related to the calibration data. Recent examples of the use of MCMC for EOS applications can be found in [Lindquist et al. \(2023\)](#) or [Brown et al. \(2023\)](#), and in [Robinson et al. \(2013\)](#) for fitting a linear model to shock wave-particle velocity data in particular. Another approach to uncertainty quantification (UQ) is called bootstrapping, which involves repeatedly resampling the original dataset to obtain new datasets and then fitting the model of interest to each new dataset. An example application of bootstrapping to EOS model development can be found in [Ali et al. \(2020\)](#). Bayesian and bootstrap methods both provide distributions over the parameters of interest, though the Bayesian approach naturally incorporates prior information into the distribution as we discuss later. The two methods have also been combined for calibrating an EOS model from limited simulated and experimental data ([Lindquist et al., 2024](#)).

To the best of our knowledge, the literature does not contain a tutorial on Bayesian analysis of linear shock compression data or a closed-form Bayesian analysis. Our analysis relies on the fact that if a certain prior distribution on the linear model and measurement error parameters is assumed, then the marginal posterior distribution of the linear model parameters is a bivariate  $t$ -distribution and this distribution can be sampled directly. This result is well-known in the statistics literature - details can be found in [Gelman et al. \(1995, Ch. 14\)](#), [Rencher and Schaalje \(2008, Ch. 11\)](#), or [Banerjee \(2008\)](#), for example - but it does not appear to have been applied to quantifying uncertainty in shock wave EOS. Alternatively, MCMC can be used to sample from the posterior distribution of the linear model parameters, but this approach is more computationally expensive and does not provide the mean and covariance matrix of the posterior distribution in closed-form. Bootstrapping is another option for performing uncertainty quantification of linear models, and we provide a comparison of the Bayesian and bootstrapping approaches for completeness. One difference is that the Bayesian analysis produces a distribution that quantifies uncertainty in the linear model parameters for the available dataset, whereas bootstrapping produces a distribution that quantifies uncertainty in the parameter estimates over different datasets. Linear regression is also an option for analyzing linear shock compression data; [Marsh \(1980\)](#) effectively takes this approach by reporting least squares estimates of the linear model parameters. As we will discuss, many of the linear regression estimates coincide with Bayesian estimates if a certain prior distribution is assumed, though the Bayesian modeling framework is more general due, in part, to the user-specified prior distribution.

Overall, this tutorial covers the following topics arising in shock compression analysis:

1. We show how to perform a Bayesian analysis of linear shock wave-particle velocity data, including inference of the linear model parameters and validation of the model. To make the tutorial self-contained, we provide a derivation of the previously mentioned posterior bivariate  $t$ -distribution of the coefficients of the linear relation between shock wave and particle velocity.
2. We show how to sample the posterior distribution of the linear model parameters and how to propagate those samples through the Rankine-Hugoniot equations to obtain Hugoniot curves in the pressure-volume plane.
3. We apply this methodology to published data on argon, copper, and nickel from [Marsh \(1980\)](#).
4. We provide a detailed example comparing this methodology to bootstrapping.

Furthermore, the plots and tables in this paper can be reproduced with the code and data in the repository [github.com/llnl/BALSCD](https://github.com/llnl/BALSCD). The repo name, BALSCD, is an acronym that stands for Bayesian Analysis of Linear Shock Compression Data. This repository also includes a script that can be used to perform the Bayesian and bootstrap analysis on new datasets. For example, the script can be used to analyze datasets on pyrolusite, serpentine, and toluene from [Marsh \(1980\)](#) that are contained in the repository but are not analyzed in this paper. Additional shock wave-particle velocity datasets can be found in [Marsh \(1980\)](#) or [Levashov et al. \(2004\)](#).

We emphasize that Bayesian analysis of linear models is well-established, so this paper does not develop new methodology or provide novel statistical content; instead, it aims to be a tutorial on the application of Bayesian modeling and calibration to analyzing linear shock compression data. To summarize the Bayesian analysis, the posterior distribution of the linear model parameters is first identified as a bivariate  $t$ -distribution centered at the least squares estimate. Samples are then drawn from this  $t$ -distribution and used to compute the shock wave-particle velocity Hugoniot curve, which is in-turn used to solve the Rankine-Hugoniot equations for pressure and volume. The method is shown to produce Hugoniot curves in the pressure-volume plane that are consistent with experimental measurements and to be less sensitive than bootstrapping to the point in the copper dataset that has the largest particle velocity. This tutorial is not a full uncertainty quantification analysis of linear models for shock compression data; for example, we do not consider the issue of model form error. Instead, its focus is on presenting Bayesian calibration of the linear model parameters in a pedagogical format.

The outline of this paper is as follows. Section 2 presents the motivating problem in more detail and introduces the data that is analyzed throughout this paper. Section 3 shows how to fit this data in a Bayesian framework. Section 4 shows how to use the results from the Bayesian analysis to sample Hugoniot curves in the pressure-volume plane. Section 5 compares the Bayesian approach with bootstrapping and linear regression. Section 6 discusses Bayesian methods more generally, offers guidance on choosing a method, and notes several topics not covered in this tutorial. Section 7 concludes the paper and suggests directions for future work. We emphasize that all of the figures and tables in this paper can be created by running the code in the accompanying repository. Reading the code in parallel with this paper, specifically the script `recreate_paper_results.py`, can reinforce the main ideas and notation.

## 2 Motivating Problem

In a shock compression experiment, a shock wave moves through a material with velocity  $U_s$  and the material behind the shock front moves with velocity  $U_p$ , as illustrated in Fig. 1. Each experiment produces a single shock wave and particle velocity measurement, the latter being the velocity of the material behind the shock front. In words, our goal is to perform uncertainty quantification on the parameters of a linear Hugoniot model relating shock wave velocity to particle velocity. The linear model is usually written as

$$U_s = C_0 + S U_p, \quad (1)$$

where the intercept,  $C_0$ , is the bulk sound velocity and the slope,  $S$ , is the instantaneous rate of change of the shock wave velocity with the particle velocity. Hence,  $C_0$  has the same units as  $U_s$  and  $U_p$ , and  $S$  is unitless. Note that not all shock wave-particle velocity datasets display a linear relationship; for example, Ahrens (1993) notes that the linear model is used when the material does not undergo a significant phase transition. However, our analysis only considers datasets that are linear. Additional details on shock compression physics and experiments can be found in Nellis (1990), Ahrens (1993), Forbes (2012), and Marsh (1980).

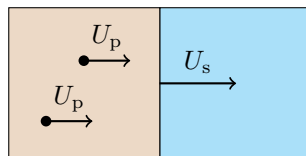


Figure 1: Illustration of a shock compression experiment where the particle velocity is  $U_p$  and the shock wave velocity is  $U_s$ . The centerline represents the shock front and the brown and blue regions are the material behind and in front of the shock front, respectively. The black circles represent the material behind the shock front and the arrows indicate the velocities.

In order to perform a statistical analysis of the linear model in Eq. (1), we rewrite the model using standard linear model notation and include a measurement error term. Assume there are  $n$  shock wave and particle velocity measurements, denoted  $Y_1, Y_2, \dots, Y_n$  and  $x_1, x_2, \dots, x_n$ , respectively, with  $n \geq 3$ . The published datasets do not provide separate uncertainties for the shock wave and particle velocities,

so we consider a single measurement error term on the shock wave velocity that effectively captures all sources of experimental uncertainty. A linear statistical model for the relationship between the shock wave and particle velocities is therefore

$$Y_i = C_0 + Sx_i + \epsilon_i \quad (2)$$

for  $i = 1, \dots, n$ , where the  $\epsilon_i$  are measurement errors that are modeled as independent and identically distributed normal random variables that have mean zero and variance  $\sigma^2$ . This model can be rewritten in matrix notation as

$$Y = X\beta + \epsilon, \quad (3)$$

where  $\beta = (C_0, S)'$  denotes the Hugoniot parameters of interest,  $Y = (Y_1, \dots, Y_n)'$  denotes the shock wave velocity measurements,  $X$  is an  $n \times 2$  design matrix whose first column is all ones and whose second column is  $(x_1, \dots, x_n)'$ , and  $\epsilon = (\epsilon_1, \dots, \epsilon_n)'$ . The main statistical notation used in this paper is summarized in Table I.

Table I: Statistical notation.

Notation	Meaning
$\beta = (C_0, S)'$	Hugoniot parameters
$\hat{\beta} = (\hat{C}_0, \hat{S})'$	Estimate of $\beta$
$n$	Number of measurements
$Y = (Y_1, \dots, Y_n)'$	Shock wave measurements
$x_i$	$i$ th particle velocity for $i = 1, \dots, n$
$X$	Design matrix
$\epsilon_i$	$i$ th measurement error
$\sigma^2$	Variance of measurement error
$p(\beta, \sigma^2)$	Prior distribution
$p(\beta, \sigma^2 Y)$	Joint posterior distribution of $\beta$ and $\sigma^2$
$p(\beta Y)$	Marginal posterior distribution of $\beta$
$s^2$	Estimate of $\sigma^2$
$\Sigma = s^2(X'X)^{-1}$	Scale matrix of posterior $t$ -distribution
$\nu = n - 2$	Degrees of freedom
$t_2(\hat{\beta}, \Sigma, \nu)$	Posterior $t$ -distribution of $\beta$
$\alpha \in (0, 1)$	Probability level
$t_{\alpha, \nu}$	$\alpha$ th quantile of a univariate $t$ -distribution
$x_*$	An arbitrary particle velocity
$p(\tilde{y} Y)$	Posterior predictive distribution

The objective of our Bayesian analysis is to determine the probability distribution of the linear model parameters,  $C_0$  and  $S$ , conditioned on the experimental measurements, or  $p(\beta|Y)$ . As a by-product, we will also be able to infer the probability distribution of the measurement error variance,  $\sigma^2$ , conditioned on the experimental measurements, or  $p(\sigma^2|Y)$ . These conditional probability distributions characterize the uncertainty in the model parameters given the experimental data, and can be used to answer questions such as ‘‘Given our data, what is the probability that  $S$  is contained in the interval (1.5, 1.6)?’’.

We illustrate the Bayesian analysis using shock compression data on argon, copper, and nickel from Marsh (1980). The data are shown in Fig. 2 along with least squares fits. These datasets were compiled from other sources that are referenced in Marsh (1980). For the copper dataset, 114 points are from impedance matching experiments, 26 are from shock and particle velocity experiments, three are from shock and free surface velocity experiments, and one is from a sound speed experiment. The copper dataset originally had 115 points from impedance matching experiments, but we removed one duplicate point because it is unlikely that two experiments produced the exact same measurements. The point with the largest particle velocity is from a shock and free surface velocity experiment. All of the points in the argon dataset are from impedance matching experiments. For the nickel dataset, 18 of the points are from impedance matching experiments and one point is from a sound speed experiment. The sound speed experiments are those with  $U_p = 0$ . Note that the points generally fall on a straight line, but some

points deviate from this line in a way that appears to be consistent with random noise or measurement error.

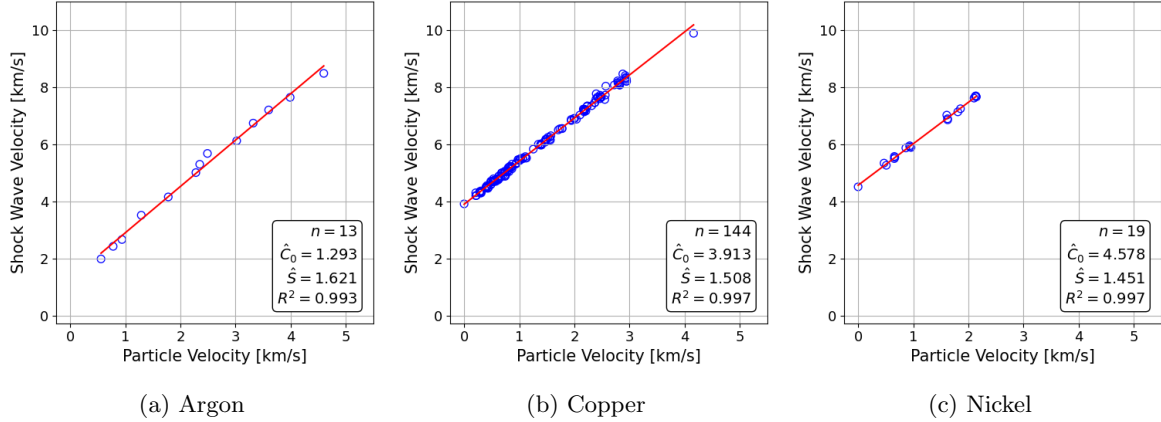


Figure 2: Shock Hugoniot data for three materials from Marsh (1980). The lower right hand corner indicates the number of points,  $n$ , in each dataset, along with the least squares estimates of  $C_0$  and  $S$  and the  $R^2$  statistic. Note that the axes are not drawn to scale.

The linear model fits in Fig. 2 are computed using the least squares estimate of  $\beta$ ,

$$\hat{\beta} = (X'X)^{-1}X'Y, \quad (4)$$

where  $\hat{\beta} = (\hat{C}_0, \hat{S})'$ . This expression is derived in Rencher and Schaalje (2008, Theorem 7.3a) by minimizing the error sum of squares, or

$$\hat{\beta} = \arg \min_{\beta} (Y - X\beta)'(Y - X\beta). \quad (5)$$

The predicted shock wave velocity at a particle velocity  $x_*$  is then given by  $\mathbf{x}'_*\hat{\beta}$ , where  $\mathbf{x}_* = (1, x_*)'$ . The  $R^2$  statistic shown in the plots is a measure of the strength of the linear correlation between the shock wave and particle velocities. An  $R^2$  equal to one would imply that shock wave velocity is a linear function of particle velocity, whereas a value of  $R^2$  equal to zero would imply that there is no correlation between shock wave and particle velocity. Hence, the  $R^2$  values near one indicate that the two velocities are almost perfectly correlated.

A linear model can be fit to the shock Hugoniot data with least squares as shown in this section, but this model is limited since it assumes that the  $\beta$  parameters are constants. This assumption makes it difficult to incorporate certain types of prior information about  $\beta$  into its estimate, such as a belief that  $C_0$  is between two and four and close to three. One approach to including this information is to model  $C_0$  with a normal distribution centered at three and with a standard deviation of 0.5. This example suggests that a better approach is to model  $\beta$  as a realization from a probability distribution that reflects prior knowledge or beliefs about  $\beta$ . Inference of  $\beta$  is then accomplished by updating this probability distribution with experimental data. This procedure is called Bayesian inference because it relies on Bayes' rule, as described next.

### 3 Bayesian Analysis

The Bayesian linear regression model assumes that the observed shock wave velocities are generated from the linear model in Eq. (3), and is made Bayesian by assuming that  $\beta$  and  $\sigma^2$  are random variables. There are two joint distributions over  $\beta$  and  $\sigma^2$  that are of interest. First, there is the distribution  $p(\beta, \sigma^2)$ , which is called the prior distribution since it reflects beliefs about these parameters that are independent of the experimental data. That is, the beliefs are formulated before the data are collected. The second distribution of interest is  $p(\beta, \sigma^2|Y)$ , which is called the posterior distribution since it is the

conditional distribution of  $\beta$  and  $\sigma^2$  given the shock wave velocity data. This material and additional details on Bayesian analysis of linear models can be found in [Gelman et al. \(1995, Ch. 14\)](#), [Rencher and Schaalje \(2008, Ch. 11\)](#), or [Banerjee \(2008\)](#), for example.

Performing a Bayesian analysis requires specifying a prior distribution and computing the resulting posterior distribution. By Bayes' rule, the posterior distribution is given by

$$p(\beta, \sigma^2|Y) = \frac{p(Y|\beta, \sigma^2)p(\beta, \sigma^2)}{p(Y)}, \quad (6)$$

where

$$p(Y) = \int p(Y|\beta, \sigma^2)p(\beta, \sigma^2) d\beta d\sigma^2 \quad (7)$$

is called the model evidence. Note that the model evidence does not depend on  $\beta$  and  $\sigma^2$ , the parameters of interest, since they are integrated out using the law of total probability. Hence, we ignore the model evidence and focus instead on the two terms in the numerator of Eq. (6). The first term follows from the Gaussian measurement model in Eq. (3) as

$$p(Y|\beta, \sigma^2) = \frac{1}{(2\pi\sigma^2)^{n/2}} \exp\left(-\frac{1}{2\sigma^2}(Y - X\beta)'(Y - X\beta)\right). \quad (8)$$

This term is called the likelihood of the model when it is written as a function of  $(\beta, \sigma^2)$ , as in  $L(\beta, \sigma^2)$ , and captures the contribution of the data to the posterior distribution. The second term is the prior distribution that is selected by the analyst. We employ the prior distribution

$$p(\beta, \sigma^2) \propto \frac{1}{\sigma^2}, \quad (9)$$

which is called improper because it does not integrate to one and therefore is not an actual probability distribution. However, this prior distribution can be used because it leads to a posterior distribution that integrates to one. This prior distribution is commonly used for several reasons. First, it does not depend on  $\beta$ , and therefore it does not bias the posterior distribution towards any particular values of  $\beta$ . The prior distribution is said to be non-informative for this reason; an analysis with an informative, normal prior distribution on  $\beta$  is given in [Appendix H](#). Second, it encodes a belief that the measurement error variance is small since the prior distribution decreases as  $\sigma^2$  increases. Third, for linear models with likelihood given by Eq. (8), this prior distribution leads to a posterior distribution that is available in closed-form and can be sampled easily, as described next.

The joint posterior distribution of the physics and measurement error parameters is derived in [Appendix B](#), in closed-form and up to a normalizing constant, as

$$p(\beta, \sigma^2|Y) \propto p(\beta|\sigma^2, Y)p(\sigma^2|Y), \quad (10)$$

where

$$p(\beta|\sigma^2, Y) = \frac{1}{2\pi\sigma^2|X'X|^{-1/2}} \exp\left(-\frac{1}{2\sigma^2}(\beta - \hat{\beta})'(X'X)(\beta - \hat{\beta})\right) \quad (11)$$

and

$$p(\sigma^2|Y) = \frac{b^a}{\Gamma(a)} \frac{1}{(\sigma^2)^{a+1}} \exp\left(-\frac{b}{\sigma^2}\right) \quad (12)$$

for  $a = (n - 2)/2$  and  $b = (n - 2)s^2/2$ . That is, the distribution of  $\beta$  given  $\sigma^2$  and  $Y$  is a normal distribution with mean  $\hat{\beta}$  and covariance matrix  $\sigma^2(X'X)^{-1}$ , and the marginal posterior distribution of  $\sigma^2$  is an inverse gamma (IG) distribution with shape parameter  $a$  and scale parameter  $b$ . This shows that the joint posterior distribution is a normal-inverse-gamma distribution. [Figure 11](#) in [Appendix D](#) shows the posterior distribution of  $\sigma^2$  for the datasets considered in this paper.

The interpretation of  $p(\beta|\sigma^2, Y)$  is that if  $\sigma^2$  is known, then the posterior distribution of  $\beta$  is normal. This hierarchical factorization of the joint posterior distribution suggests that one way to sample a  $\beta$  from its marginal posterior distribution is to first sample  $\sigma^2 \sim IG(a, b)$  following Eq. (12) and then to sample  $\beta \sim N(\hat{\beta}, \sigma^2(X'X)^{-1})$  following Eq. (11). Since the samples of  $\beta$  and  $\sigma^2$  are from the joint

posterior distribution of  $(\beta, \sigma^2)$ , they can be used for simulating synthetic data or for estimating integrals using Monte Carlo. For example, the probability that  $C_0$  is greater than 4 can be estimated as

$$N^{-1} \sum_{i=1}^N I\{C_0^{(i)} > 4\}, \quad (13)$$

where  $\beta^{(i)} = (C_0^{(i)}, S^{(i)})'$  is the  $i$ th of  $N$  samples of  $\beta$  and  $I\{C_0^{(i)} > 4\}$  is an indicator function that equals one if  $C_0^{(i)} > 4$  and equals zero otherwise.

Now, our goal is to obtain the marginal posterior distribution of  $\beta$ , the physics parameters of interest, without the nuisance parameter  $\sigma^2$  related to the experimental measurements. To this end, the marginal posterior distribution of  $\beta$  is obtained by integrating  $\sigma^2$  out of the full posterior distribution,  $p(\beta, \sigma^2|Y)$ , and is given in closed-form as

$$p(\beta|Y) = \frac{\Gamma(n/2)}{\Gamma(\nu/2)\nu\pi|\Sigma|^{1/2}} \left[ 1 + \frac{1}{\nu}(\beta - \hat{\beta})'\Sigma^{-1}(\beta - \hat{\beta}) \right]^{-n/2}, \quad (14)$$

which is the density of a bivariate  $t$ -distribution with  $\nu = n - 2$  degrees of freedom, mean  $\hat{\beta}$ , and scale matrix

$$\Sigma = s^2(X'X)^{-1}, \quad (15)$$

where

$$s^2 = \frac{1}{\nu}(Y - X\hat{\beta})'(Y - X\hat{\beta}) \quad (16)$$

is an estimate of the variance of the measurement errors and called the sample variance; see [Appendix A](#) for a review of the multivariate  $t$ -distribution. The marginal posterior distribution of  $\beta$  can also be expressed using the shorthand notation

$$\beta|Y \sim t_2(\hat{\beta}, \Sigma, \nu). \quad (17)$$

The mean of the marginal posterior distribution of  $\beta$ , called the posterior mean, is also the least squares estimate of  $\beta$ , or

$$E(\beta|Y) = \hat{\beta}. \quad (18)$$

The covariance matrix of the marginal posterior distribution of  $\beta$  is

$$\text{Var}(\beta|Y) = \frac{\nu}{\nu - 2}\Sigma, \quad (19)$$

which requires  $n > 4$  and is not the scale matrix,  $\Sigma$ , but closely approximates the scale matrix for large  $n$ . A derivation of the marginal posterior distribution of  $\beta$  and the posterior mean and covariance matrix of the distribution are given in [Appendix C](#). Note also that  $\hat{\beta}$  maximizes the posterior distribution in Eq. (14), and so is called the maximum a posteriori (MAP) estimate of  $\beta$  in a Bayesian context. Overall, the posterior distribution of  $\beta$  is in closed-form, the posterior mean and variance of  $\beta$  are available in closed-form, and samples from the posterior distribution of  $\beta$  can be obtained exactly.

A key point of this tutorial is that the posterior distribution of  $\beta$  is available in closed-form and is given by Eq. (17). To demonstrate the utility of this result, Fig. 3 shows the  $t$ -distribution of  $C_0$  implied by Eq. (17) and a histogram of samples from this distribution obtained with the two-step algorithm given above. As expected, there is close agreement between the analytic posterior distribution and histogram of the samples from the posterior distribution. Both distributions are useful, though. In particular, the analytic distribution provides closed-form expressions for the mean and covariance matrix of the  $C_0$  and  $S$  parameters, whereas the samples can be used for Monte Carlo calculations, as noted previously in this section. Note also that in this and subsequent figures, the axis labels are  $c_0$  or  $s$  instead of  $C_0$  or  $S$ . The distinction is that  $C_0$  and  $S$  are random variables, whereas  $c_0$  and  $s$  refer to values these random variables can take on.

Figure 4 shows the posterior distribution of  $\beta$  for the three datasets considered in this paper. Two trends are immediately apparent. First, copper has the most concentrated posterior distribution, followed by nickel and then argon. This occurs because the posterior variance tends to decrease as  $n$  increases,

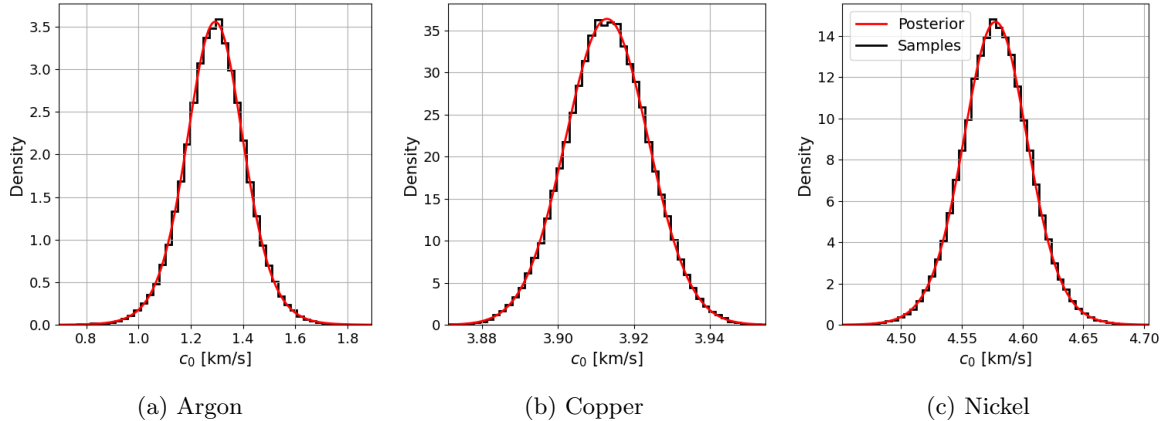


Figure 3: The marginal posterior distribution of  $C_0$  and a histogram of samples drawn from this distribution. The analytic distribution is useful because it fully characterizes the uncertainty in the Hugoniot model parameters, whereas the samples are useful for Monte Carlo and uncertainty propagation.

and copper has the most observations. To see why the variance decreases with  $n$ , note that the  $(X'X)^{-1}$  term in the posterior covariance matrix is (Rencher and Schaalje, 2008, Ex. 7.3.2a)

$$(X'X)^{-1} = \frac{1}{\sum_i (x_i - \bar{x})^2} \begin{pmatrix} n^{-1} \sum_i x_i^2 & -\bar{x} \\ -\bar{x} & 1 \end{pmatrix}, \quad (20)$$

where  $x_i$  is the  $i$ th particle velocity and  $\bar{x}$  is the mean of the  $x_i$ . Now, the denominator of the fraction increases with  $n$  while the non-constant terms in the matrix are means and therefore tend to stay approximately constant with  $n$ , so that overall the terms in this matrix trend towards zero. Second, the posterior correlation between  $C_0$  and  $S$  is negative since the off-diagonal terms in Eq. (20) are  $-\bar{x}$  and the mean particle velocity,  $\bar{x}$ , is positive. Intuitively, the correlations are negative because if  $C_0$  increases, then  $S$  has to be decreased in order for the Hugoniot line to go through the shock wave-particle velocity measurements, and conversely if  $C_0$  decreases, then  $S$  has to be increased to compensate for a smaller intercept term.

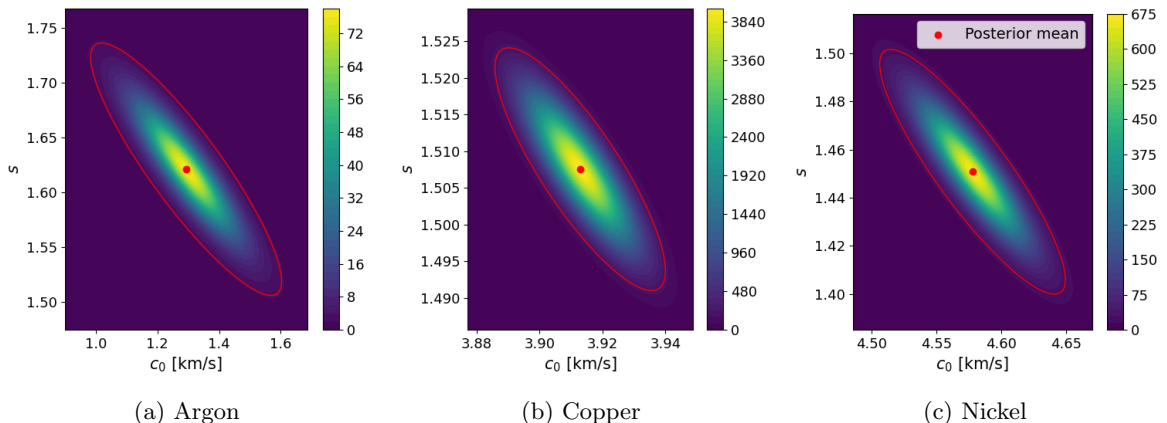


Figure 4: Posterior distributions of  $C_0$  and  $S$ . The red ellipses are 95% credible regions, meaning they contain 95% of the posterior probability.

The red ellipses in Fig. 4 are 95% credible regions for  $\beta$ , or a set of values such that the probability that  $\beta$  is contained in that region, conditioned on the experimental data, is 0.95. The credible region for  $\beta$  is elliptical by Eq. (14). A derivation of this credible region is given in Appendix G.

Similar to credible regions, an interval that contains an element of  $\beta$  with a specified probability under the posterior probability distribution is called a credible interval. For example, a 95% credible

interval for  $C_0$  is

$$(\hat{C}_0 + t_{0.025,\nu}\sigma_{11}, \hat{C}_0 + t_{0.975,\nu}\sigma_{11}), \quad (21)$$

where  $\sigma_{11}^2$  is the (1, 1)th element of  $\Sigma$  and  $t_{0.025,\nu}$  and  $t_{0.975,\nu}$  are the 0.025th and 0.975th quantiles of a  $t$ -distribution with  $\nu$  degrees of freedom. Similarly, a 95% credible interval for  $S$  is

$$(\hat{S} + t_{0.025,\nu}\sigma_{22}, \hat{S} + t_{0.975,\nu}\sigma_{22}), \quad (22)$$

where  $\sigma_{22}^2$  is the (2, 2)th element of  $\Sigma$ . In words, the probability that  $C_0$  is contained in the interval given by Eq. (21), conditioned on the experimental data, is 0.95, and the same interpretation holds for  $S$  and its credible interval. These intervals are derived in [Appendix F](#) using the fact that the marginal posterior distributions of the elements of  $\beta$  are univariate  $t$ -distributions.

For this two-dimensional posterior distribution, the univariate credible intervals are simpler to write down than the bivariate credible regions, but the credible regions are more informative since they capture the correlation between  $C_0$  and  $S$ .

Table II summarizes the posterior distribution of the  $C_0$  and  $S$  parameters for the argon, copper, and nickel datasets. The posterior mean is  $\hat{\beta}$ , the posterior standard deviations are given by the square roots of the diagonal elements of  $\nu/(\nu - 2)\Sigma$ , and the credible intervals are given by Eq. (21) and Eq. (22) for  $C_0$  and  $S$ , respectively. Note again the decrease in posterior variance as the sample size increases.

Table II: Posterior means, standard deviations, and 95% credible intervals for  $C_0$  and  $S$ .

Material	Parameter	Posterior Mean	Posterior Standard Deviation	95% Credible Interval	Units
Argon	$C_0$	1.293	0.121	(1.052, 1.535)	km/s
	$S$	1.621	0.045	(1.531, 1.711)	.
Copper	$C_0$	3.913	0.011	(3.891, 3.935)	km/s
	$S$	1.508	0.007	(1.494, 1.521)	.
Nickel	$C_0$	4.578	0.028	(4.521, 4.634)	km/s
	$S$	1.451	0.020	(1.411, 1.491)	.

This section gave an analytical expression for the posterior distribution of the  $\beta$  parameters and showed how to summarize and draw samples from this distribution. These samples can be propagated through the Rankine-Hugoniot equations to obtain Hugoniot curves in the pressure-volume plane. The posterior distribution can also be propagated analytically to obtain the distribution of the shock wave velocity as a function of the particle velocity. We continue in the next section with details on both uncertainty propagation tasks.

## 4 Uncertainty Propagation

This section covers two topics related to uncertainty propagation. First, we show how to sample Hugoniot curves in the pressure-volume plane that are consistent with the experimental data by sampling  $\beta$  from its marginal posterior distribution and propagating those samples through the non-linear Rankine-Hugoniot equations. Second, we show how to characterize uncertainty in the shock wave velocity and future shock wave velocity measurements as a function of particle velocity. The order of topics may seem backward because the previous section focused on shock wave-particle velocity data, but we chose this order of topics because the first topic only requires information about the posterior distribution presented thus far, whereas the second topic requires a new concept called the posterior predictive distribution.

The Rankine-Hugoniot equations are a set of conservation equations that relate the shock wave and particle velocities to the change in pressure, volume, and internal energy of the material. The conservation of mass equation is

$$\frac{V}{V_0} = \frac{U_s - U_p}{U_s}, \quad (23)$$

the conservation of momentum equation is

$$P - P_0 = \rho_0 U_s U_p, \quad (24)$$

and the conservation of energy equation is

$$E - E_0 = \frac{1}{2}(P + P_0)(V_0 - V), \quad (25)$$

where  $V_0$ ,  $P_0$ ,  $E_0$ , and  $\rho_0$  are the initial volume, pressure, internal energy, and density of the material ahead of the shock front, and  $V$ ,  $P$ , and  $E$  are the volume, pressure, and internal energy of the material behind the shock front. Hence, a Hugoniot curve in the pressure-volume plane can be obtained from these equations and a Hugoniot curve in the shock wave-particle velocity plane.

Hugoniot curves can be sampled in the pressure-volume plane with the following three step procedure:

1. Following [Hofert \(2013\)](#), draw a sample from the marginal posterior distribution of  $\beta$  defined in Eq. (17),

$$\beta = LZ\sqrt{\nu/W} + \hat{\beta}, \quad (26)$$

where  $Z = (Z_1, Z_2)'$  is a bivariate normal random vector with mean  $(0, 0)'$  and identity covariance matrix,  $W$  is a chi-square random variable with  $\nu = n - 2$  degrees of freedom, and  $L$  is a lower-triangular matrix obtained from the Cholesky decomposition of  $\Sigma$  and satisfies  $\Sigma = LL'$ . In Python, this procedure for sampling  $\beta$  is implemented in the `multivariate_t` class in the `scipy.stats` module.

2. Given this  $\beta$ , evaluate the corresponding Hugoniot curve in the shock wave-particle velocity plane over a grid of  $U_p$  values using Eq. (1).
3. Propagate the linear Hugoniot curve through the Rankine-Hugoniot equations, Eq. (23) and Eq. (24), to obtain a Hugoniot curve in the pressure-volume plane.

In words, these steps sample values of  $C_0$  and  $S$  from the posterior distribution and propagate those values through the Rankine-Hugoniot equations to obtain a Hugoniot in the pressure-volume plane. The procedure for sampling  $\beta$  from its marginal posterior distribution given in Sec. 3 could also be used for step 1, but the procedure given here is useful for deriving certain results later in this section. Note also that given the sampled values of  $P$  and  $V$ , the internal energy can be computed from Eq. (25) if a value of  $E_0$  is available.

Figure 5 shows 95% credible intervals for pressure as a function of volume. That is, the figure does not show individual Hugoniot curve samples, but rather a summary of their distribution. To create this plot, we first sample a large number of  $\beta$  vectors from their posterior distribution and then evaluate the corresponding shock wave-particle velocity curves over a grid of  $U_p$  values that includes the range of particle velocity measurements. The Rankine-Hugoniot equations for volume and pressure given in Eq. (23) and Eq. (24), respectively, are then evaluated taking the initial density,  $\rho_0$ , to be the average value of the initial densities in [Marsh \(1980\)](#), taking the initial volume to be one over this mean initial density, and taking the initial pressure,  $P_0$ , to be 1 bar, or  $10^{-4}$  GPa, corresponding to ambient conditions. At this point, we have a collection of curves in the pressure-volume plane, but the volumes are different for different samples of  $\beta$ , so we perform a linear interpolation step to adjust the Hugoniot curves to a common set of volumes. Finally, we compute the 0.025th and 0.975th pressure quantiles across this grid of volumes to obtain the shaded regions in Fig. 5. We see, for example, that the variability in pressure for argon can be on the order of 125 GPa for small volumes, but less than 5 GPa for large volumes; the variability in pressure is due to the non-linearity of the Rankine-Hugoniot equations. For the copper and nickel datasets, the variability in pressure is significantly less than for the argon dataset since their posterior distributions for  $\beta$  are more concentrated, as seen in Fig. 4. Note also that the points with the highest particle and shock wave velocities have the smallest volumes and highest pressures in these plots, indicating the greatest degree of compression.

The posterior distribution of  $\beta$  can also be propagated analytically through Eq. (1) to quantify uncertainty in the mean shock wave velocity at a specified particle velocity. In particular, the posterior distribution of the mean shock wave velocity at a particle velocity  $x_*$  is derived by multiplying both sides of Eq. (26) by  $\mathbf{x}'_* = (1, x_*)$  to get

$$\mathbf{x}'_*\beta = \mathbf{x}'_*LZ\sqrt{\nu/W} + \mathbf{x}'_*\hat{\beta}. \quad (27)$$

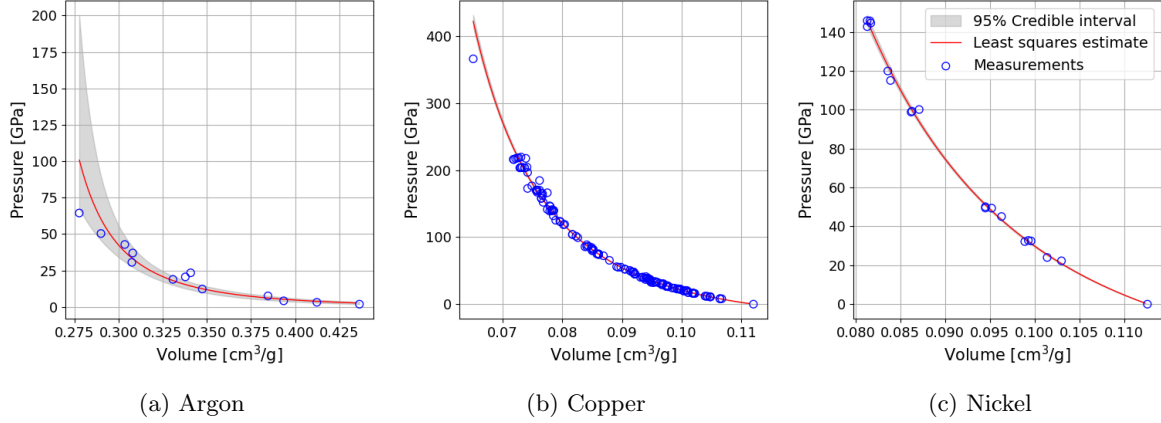


Figure 5: Credible intervals for the Hugoniot curve in the pressure-volume plane, obtained from the posterior distribution of  $C_0$  and  $S$ .

By linearity,  $\mathbf{x}'_* LZ$  is normally distributed with mean 0 and variance  $\mathbf{x}'_* \Sigma \mathbf{x}_*$ , and since every multivariate  $t$ -distribution can be expressed in the form of Eq. (26) for different choices of the scale matrix, mean vector, and degrees of freedom, it follows that the posterior distribution of  $U_s = \mathbf{x}'_* \hat{\beta}$  is a univariate  $t$ -distribution with mean  $\mathbf{x}'_* \hat{\beta}$ , scale matrix  $\mathbf{x}'_* \Sigma \mathbf{x}_*$ , and  $\nu$  degrees of freedom, written

$$U_s | Y \sim t_1(\mathbf{x}'_* \hat{\beta}, \mathbf{x}'_* \Sigma \mathbf{x}_*, \nu). \quad (28)$$

A 95% credible interval for the mean shock wave velocity is therefore

$$(\mathbf{x}'_* \hat{\beta} + t_{0.025, \nu} \sqrt{\mathbf{x}'_* \Sigma \mathbf{x}_*}, \mathbf{x}'_* \hat{\beta} + t_{0.975, \nu} \sqrt{\mathbf{x}'_* \Sigma \mathbf{x}_*}), \quad (29)$$

where again  $t_{0.025, \nu}$  and  $t_{0.975, \nu}$  are the 0.025th and 0.975th quantiles of a  $t$ -distribution with  $\nu$  degrees of freedom; as shown in Appendix J, the  $t$ -distribution converges to the normal distribution as  $n \rightarrow \infty$ , so that  $t_{0.025, \nu}$  and  $t_{0.975, \nu}$  are approximately -1.96 and 1.96 for large values of  $\nu$ , respectively. The variance term can be rewritten as

$$\mathbf{x}'_* \Sigma \mathbf{x}_* = s^2 \left( \frac{1}{n} + \frac{(x_* - \bar{x})^2}{\sum_{i=1}^n (x_i - \bar{x})^2} \right), \quad (30)$$

which increases with the distance from  $x_*$  to  $\bar{x}$  and is expected to decrease with increasing  $n$  for shock compression experiments where the particle velocities are bounded. Hence, credible intervals for the mean shock wave velocity are narrowest at the mean particle velocity and tend to shrink as the number of measurements increases.

Uncertainty in future shock wave velocity measurements is quantified with the posterior predictive distribution. If the new shock wave velocity measurement is denoted  $\tilde{Y}$ , then the posterior predictive distribution at a particular value that  $\tilde{Y}$  can take on, say  $\tilde{y}$ , is  $p(\tilde{y}|Y)$ , which is computed from the measurement distribution and posterior distribution as

$$p(\tilde{y}|Y) = \int p(\tilde{y}|\beta, \sigma^2) p(\beta, \sigma^2|Y) d\beta d\sigma^2. \quad (31)$$

As derived in Appendix E, the posterior predictive distribution at a particle velocity  $x_*$  is

$$\tilde{Y}|Y \sim t_1(\mathbf{x}'_* \hat{\beta}, s^2 + \mathbf{x}'_* \Sigma \mathbf{x}_*, \nu). \quad (32)$$

The mean of this distribution is the least squares prediction,  $\mathbf{x}'_* \hat{\beta}$ , and the scale matrix is the sum of the sample variance of the residuals,  $s^2$ , and the scale matrix of the distribution of  $U_s | Y$  given in Eq. (28). Hence, the variance of the posterior predictive distribution accounts for uncertainty from the new measurement error and from the posterior distribution of the shock wave velocity. As the number of measurements increases, the variance of the posterior predictive distribution converges to the variance of the measurement error,  $\sigma^2$ , since  $s^2$  converges to  $\sigma^2$ , and  $\mathbf{x}'_* \Sigma \mathbf{x}_*$  converges to zero from Eq. (30).

Figure 6 shows 95% credible intervals for the mean shock wave velocity and 95% prediction intervals for future shock wave velocity measurements. The latter are computed as quantiles of the posterior predictive distribution from Eq. (32) as

$$(\mathbf{x}'_* \hat{\beta} + t_{0.025, \nu} \sqrt{s^2 + \mathbf{x}'_* \Sigma \mathbf{x}_*}, \mathbf{x}'_* \hat{\beta} + t_{0.975, \nu} \sqrt{s^2 + \mathbf{x}'_* \Sigma \mathbf{x}_*}), \quad (33)$$

which differs from the credible interval given in Eq. (29) by an extra  $s^2$  in the variance term to account for measurement error. Two observations from these plots are readily apparent. First, the credible interval width decreases with the sample size, as expected from the previous discussion about the variance of the posterior predictive distribution decreasing as the number of measurements increases. This is evident comparing the credible intervals for the copper and argon datasets, which are barely visible and easy to see, respectively. Second, the prediction intervals tend to contain the shock wave velocity measurements, except for copper which has several points falling outside the prediction bands. This is not surprising since only 95% of future measurements are expected to be contained in the prediction intervals, and furthermore prediction intervals are designed to contain future measurements with some specified probability, not current measurements. Assessing prediction interval coverage on the data used to construct the posterior distribution is mainly meant as a heuristic to detect model fitting issues.

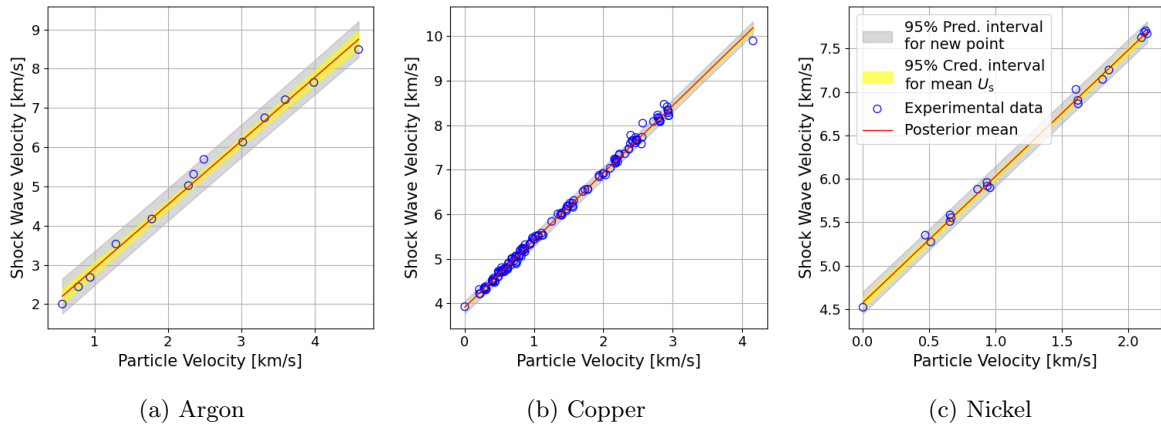


Figure 6: Credible intervals for mean shock wave velocities and prediction intervals for future shock wave velocity measurements, obtained from the posterior distributions of  $C_0$ ,  $S$ , and  $\sigma^2$ .

To validate the fitted model, we simulate shock wave velocity measurements from the posterior predictive distribution and plot them against the actual shock wave velocity measurements. This is called a posterior predictive check and is discussed more generally in Gelman et al. (2020, Sec. 6.3). Figure 7 shows the results. We see that the simulated and original measurements are close and differ by random error, which is expected since the original measurements had  $R^2$  values close to one and both simulated and real measurements are generated with measurement error. Deviation of the points from the red reference line, such as the points being systematically above or below the line, would suggest issues with the assumed linear model. Hence, these plots do not suggest a serious issue with the fitted model, such as missing a systematic bias or mis-specifying the error model. Note, however, that care needs to be taken when performing posterior predictive checks since different simulated datasets will produce different results, so it is advisable to perform posterior predictive checks with multiple sets of simulated data. Also note that there are many ways to compare real and simulated data, and that we are showing a single visual approach.

## 5 Comparison with Linear Regression and Bootstrapping

Two alternatives to the Bayesian method discussed here are linear regression and bootstrapping. This section describes these methods and compares them to Bayesian linear regression. Overall, our viewpoint is not that one method is preferred over another, but rather that they have different assumptions and interpretations, which this section aims to make clear.

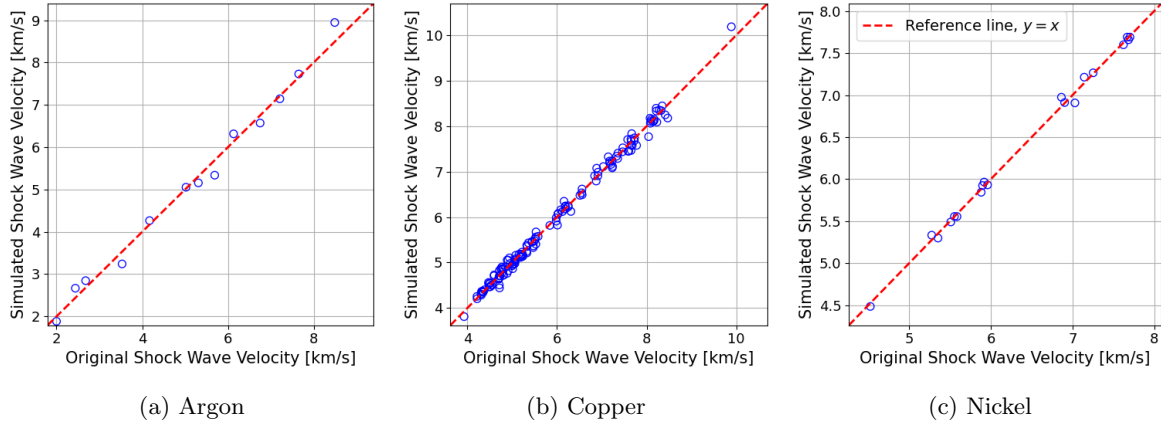


Figure 7: Posterior predictive checks comparing the actual shock wave velocity measurements to measurements simulated from the posterior predictive distribution.

The linear regression model for the shock wave velocities is given by Eq. (3), but in this case the  $\beta$  and  $\sigma^2$  parameters are treated as constants instead of random variables. Consequently, there is no prior distribution on  $\beta$  and  $\sigma^2$  in non-Bayesian linear regression. The maximum likelihood estimate (MLE) of  $\beta$  is obtained by maximizing the likelihood given in Eq. (8), which results in the estimate  $\hat{\beta}$  given by Eq. (5). The MLE is normally distributed with mean  $\beta$  and covariance matrix  $\sigma^2(X'X)^{-1}$ , written

$$\hat{\beta} \sim N(\beta, \sigma^2(X'X)^{-1}). \quad (34)$$

In practice,  $\sigma^2$  is not known and so is replaced with the sample variance,  $s^2$ . This leads to  $t$ -distributions for the elements of  $\hat{\beta}$  that coincide with the marginal posterior distributions of  $\beta$ . Hence, confidence intervals for the elements of  $\beta$  are the same as the credible intervals obtained in the Bayesian framework. However, confidence and credible intervals have different interpretations. In non-Bayesian linear regression,  $C_0$  is treated as a fixed but unknown parameter, and a 95% confidence interval for  $C_0$  is constructed such that, under repeated sampling, approximately 95% of such intervals would contain the true value of  $C_0$ . The same interpretation applies to the slope parameter  $S$ . In contrast, with Bayesian linear regression,  $\beta$  is treated as a random vector, and a 95% credible region is interpreted as the region that, conditional on the data, contains  $\beta$  with probability 0.95. These differing interpretations should be considered when choosing to summarize uncertainty with confidence or credible intervals. Furthermore, the intervals will not be equal if other prior distributions are placed on the model parameters.

Bootstrapping is another approach to inference that relies on creating new datasets that have similar statistical properties to the original dataset. The approach we take, called non-parametric bootstrapping, involves creating synthetic datasets by sampling the original shock wave-particle velocity measurement pairs with replacement  $n$  times. A  $\hat{\beta}$  is computed for each synthetic dataset, which results in a sampling distribution of estimates of  $C_0$  and  $S$ , referred to as a bootstrap distribution. This method of bootstrapping is called non-parametric since the new datasets are not generated from a Gaussian parametric model. In contrast, a parametric bootstrap distribution of  $\hat{\beta}$  is generated by simulating new datasets from the Gaussian model fit to the original data, and then computing  $\hat{\beta}$  for each new dataset. Other bootstrap methods have also been developed, such as the Bayesian bootstrap (Rubin, 1981), but we do not provide details here on these alternatives. More background on bootstrapping can be found in Hesterberg (2011) or DiCiccio and Efron (1996), for example.

Figure 8 compares the bootstrap distribution of  $\hat{S}$  with the posterior distribution of  $S$  for the argon, copper, and nickel datasets. Note that the bootstrap distributions are not necessarily centered around  $\hat{S}$  and can be asymmetric, as seen for the nickel dataset. In contrast, the posterior distributions have mean  $\hat{S}$  and are symmetric since they are  $t$ -distributions. The bootstrap distribution of  $\hat{S}$  also has a visibly larger variance than the posterior distribution of  $S$  for copper, though the variances appear much closer for argon and nickel. The means, standard deviations, and percentile confidence intervals for the bootstrap distributions are given in Table III; the percentile confidence intervals are computed by

taking the 2.5th and 97.5th percentiles of the bootstrap samples of  $\hat{C}_0$  and  $\hat{S}$ . In general, the bootstrap statistics agree up to the second decimal with the posterior statistics given in Table II, with some larger differences, mainly for the argon dataset, which is the smallest dataset. Figure 14 in Appendix I shows bootstrap confidence intervals on the mean shock wave velocity and prediction intervals on new shock wave measurements.

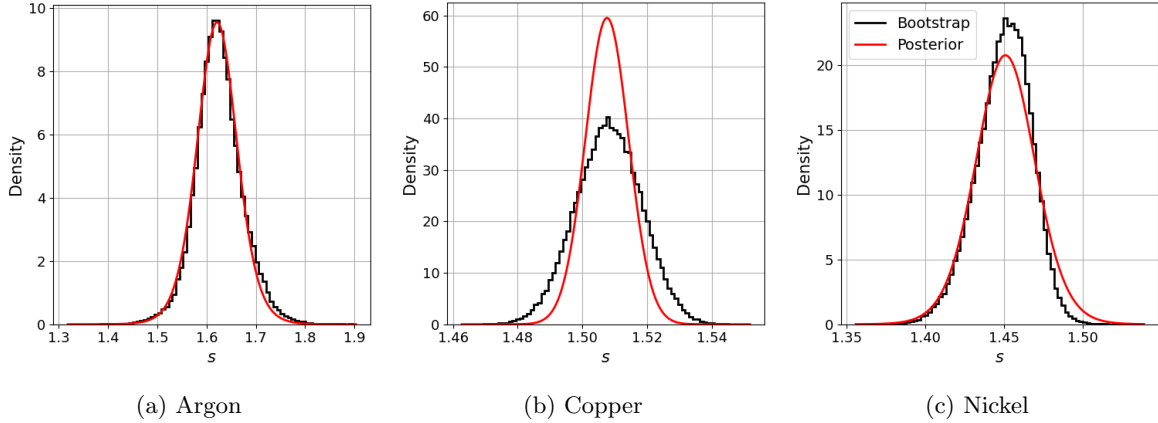


Figure 8: Bootstrap distributions of  $\hat{S}$  and posterior distributions of  $S$ .

Table III: Bootstrap means, standard deviations, and 95% percentile confidence intervals for  $C_0$  and  $S$ .

Material	Parameter	Bootstrap Mean	Bootstrap Standard Deviation	95% Percentile Confidence Interval	Units
Argon	$C_0$	1.297	0.122	(1.106, 1.588)	km/s
	$S$	1.625	0.049	(1.530, 1.727)	.
Copper	$C_0$	3.912	0.012	(3.890, 3.936)	km/s
	$S$	1.508	0.010	(1.488, 1.528)	.
Nickel	$C_0$	4.579	0.026	(4.533, 4.635)	km/s
	$S$	1.450	0.017	(1.413, 1.481)	.

A key difference between the form of bootstrapping employed here and the Bayesian approach is that the bootstrap distribution of  $\hat{\beta}$  is obtained by resampling the original dataset, whereas the posterior distribution of  $\beta$  is obtained holding the dataset fixed. For each bootstrap dataset,  $\hat{\beta}$  is computed as in Eq. (5), which is justified assuming Gaussian measurement errors, but the distribution of the  $\hat{\beta}$  resulting from the bootstrap procedure is not a bivariate  $t$ -distribution. This implies that the bootstrap confidence and prediction intervals are not  $t$ -distributed, although the posterior distribution summary statistics in Table II and bootstrap distribution summary statistics in Table III often agree to one or two decimal places.

Bootstrap distributions can also be more sensitive to individual points than posterior distributions. Figure 9 shows the bootstrap distributions and posterior distributions of  $S$  for the copper dataset with and without the point that has the largest particle velocity. This is the point that has a particle velocity greater than 4 km/s in Fig. 2b. Removing this point increases the mean of the bootstrap and posterior distributions by about 0.01 km/s, but decreases the variance of the bootstrap distribution. The variance of the bootstrap distribution is larger when the point is included in the original dataset because the point may still be excluded from some of the resampled datasets due to random chance. In contrast, the variance of the posterior distribution appears similar whether the point is included or not because the posterior distribution quantifies the uncertainty in  $S$  while holding the dataset fixed.

A point to emphasize with non-parametric bootstrapping is that due to the resampling process, a  $\hat{\beta}$  computed from a new dataset is likely to not be informed by all the measurements in the original dataset. For example, if a dataset consists of  $n = 10$  shock wave and particle velocity measurements,

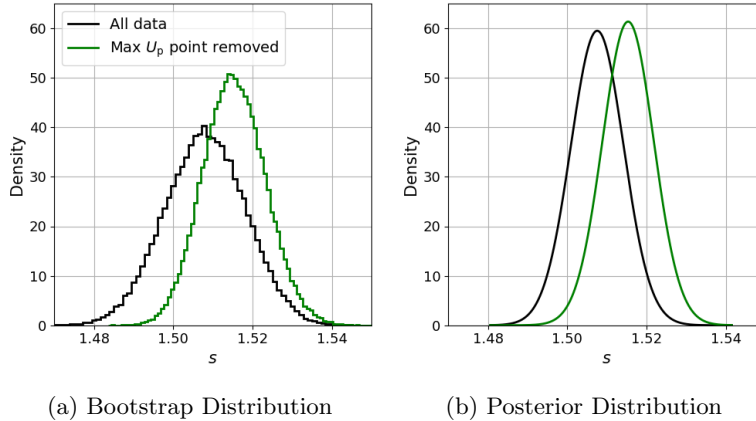


Figure 9: Bootstrap distributions of  $\hat{S}$  and posterior distributions of  $S$  for the complete copper dataset and for the dataset with the point that has the largest particle velocity removed.

then each bootstrap sample of  $\hat{\beta}$  will be based on a random resampling, with replacement, of those ten measurements, and therefore will exclude a specified measurement with probability  $0.9^{10} \approx 0.35$ . This outcome is expected with bootstrapping, and is offset by the specified measurement being included in other bootstrap samples of  $\hat{\beta}$ . In contrast, in the Bayesian approach, each sample of  $\beta$  obtained from sampling the posterior distribution of  $\beta$  is informed by each measurement in the original dataset.

One advantage of the bootstrap for this application is that it does not make any assumptions about the distribution of the measurement errors or require a prior distribution. In contrast, the Bayesian approach assumed independent, Gaussian distributed measurement errors and a non-informative prior distribution on the model parameters. If the distributional assumptions made in the Bayesian analysis lead to a model that is inconsistent with the data, then the sampled Hugoniot curves in the pressure-volume plane will also be inconsistent with the data. Given the advantages and disadvantages of the two methods, there is no clear decision rule for deciding whether to analyze shock compression data using a bootstrapping or Bayesian approach. In the EOS context, we suggest validating the uncertainty quantification from either method by comparing predictions from the sampled Hugoniot curves to observables, and also considering the interpretation of the uncertainty quantification produced by each method. If there is prior information about the linear model parameters or the parameters can be considered to be random variables, then a Bayesian analysis may be a better approach. Alternatively, if there is no prior information about the parameters or if it is preferred to treat the parameters as fixed but unknown constants, then bootstrapping is likely to be more appealing.

It is also worth noting that both bootstrapping and the Bayesian approach presented here are computationally inexpensive. The Bayesian analysis requires sampling from a bivariate  $t$ -distribution, which was shown in Sec. 3 to require sampling from a bivariate normal and chi-square distribution. Bootstrapping, in comparison, requires resampling the original dataset multiple times and fitting a least squares line to each of the new datasets. For the three datasets considered in this paper, this resampling and estimation procedure was performed 100,000 times, and the total time for performing the analysis on a standard laptop was approximately 25 seconds.

## 6 Discussion

This paper analyzed a simple linear model that had a closed-form posterior distribution due to the choice of Gaussian likelihood and improper prior distribution. More generally, the posterior distribution will be normal-inverse-gamma distributed as long as the prior distribution is also from the normal-inverse-gamma distribution. This allows more informative prior distributions to be specified for  $C_0$  and  $S$ . For example, if  $C_0$  and  $S$  are believed to be independent, then their prior distribution can be set to a bivariate normal distribution with a correlation of zero. These choices are ultimately subjective, but are helpful when there is limited data or when there is subject matter expertise that can be brought into

the analysis.

In general, posterior distributions can be sampled from approximately or computed numerically when they cannot be sampled directly or are not analytically available. This would occur for our regression model if the prior distribution was not a normal-inverse-gamma distribution, for example. One approach is to use an iterative, probabilistic algorithm called Markov Chain Monte Carlo (MCMC) to obtain approximate samples from the posterior distribution (Gelman et al., 1995, Ch. 11). The `emcee` package in Python is a popular choice for implementing MCMC (Foreman-Mackey et al., 2013), though care should be taken if the number of parameters to infer is large (Huijser et al., 2022). An MCMC algorithm called a Gibbs sampler can also be used to draw samples from the posterior distribution of the linear model parameters, as described in Chib (2001, Sec. 8.3). Note that these MCMC algorithms produce a sequence of correlated samples from the posterior distribution, whereas the direct sampling methods presented in this paper produce independent samples. Alternatively, since the linear regression model examined in this paper only has three parameters, the posterior distribution can be evaluated on a three-dimensional grid. That is, the prior distribution is multiplied by the likelihood for each grid cell to obtain the non-normalized posterior distribution, and then these values are normalized to sum to one to approximate the actual posterior distribution.

This discussion highlights the fact that the Bayesian paradigm offers great flexibility in terms of modeling choices and inferential procedures. Some analysts will view this flexibility as a strength since it allows them to examine a range of models and tailor the inferential approach to the model. Other analysts may view this flexibility as a nuisance and prefer to stick to a general computational method that works for a broad class of Bayesian models. Overall, using a more general approach than necessary is not problematic, as long as the same posterior distribution is computed or sampled. For example, MCMC can be used to sample the posterior distribution of  $(\beta, \sigma^2)$  for the Bayesian linear model presented here, and it will be relatively inefficient compared to sampling the actual normal-inverse-gamma posterior distribution directly, but both approaches target the same posterior distribution.

Several important topics were not covered in this tutorial but are now briefly mentioned for completeness:

1. In many scientific contexts, the model fit to the data is an approximation, and this approximation can introduce systematic error. For example, Brynjarsdóttir and O'Hagan (2014) gives an example of a model for work that always predicts less than the actual work. A possible explanation for this systematic discrepancy is that the model to be calibrated is missing a friction term. This model discrepancy is then modeled using a Gaussian process, which is also inferred while performing Bayesian calibration. The shock wave-particle velocity data considered here are linear, as indicated by the  $R^2$  values close to one, so that this source of error did not require consideration. However, other shock wave-particle velocity datasets in Marsh (1980) are non-linear and could be analyzed with this Gaussian process model approach.
2. The particle velocity measurements were assumed to be known exactly, but it is possible to account for particle velocity measurement error in the Bayesian modeling and calibration framework. The resulting posterior distribution is no longer available in closed-form, but it can be sampled from using MCMC; see Carroll et al. (2006, Ch. 9) for details and examples. In general, the effect of observing particle velocities with measurement error will be to flatten the regression line, which is called attenuation (Carroll et al., 2006, Ch. 3). Celliers et al. (2005) provides a non-Bayesian analysis of systematic uncertainty in impedance matching experiments.
3. A common criticism of Bayesian analysis is that it is subjective in the sense that the analyst chooses the prior distribution, and different results can be obtained with different prior distributions. This issue can be mitigated by performing a prior sensitivity analysis, as discussed in a different context in Gelman et al. (2020, Sec. 5.9), for example. For our purposes, a prior sensitivity analysis could investigate the posterior distribution of  $\beta$  assuming a normal prior distribution on  $\beta$  with a large variance. The difficulty with assuming a normal prior distribution on  $\beta$  is specifying the mean of the distribution, which we effectively avoided by choosing a non-informative prior distribution.
4. If a shock wave-particle velocity dataset includes a phase change, then the relationship between the velocities may be piecewise linear with the change in slope occurring at the phase change. Bayesian

methods can still be used to calibrate this model by including both slopes and the location of the change in slope in the set of unknown parameters, and then sampling the posterior distribution of these parameters using MCMC. See Fig. 16 in [Duvall and Graham \(1977\)](#) for an example of shock wave-particle velocity data that suggests a phase transition due to a deviation from linearity at large shock wave velocities.

5. This paper assumed that shock wave velocity was linearly related to particle velocity, but quadratic and cubic models can also be found in the literature. For example, [Root et al. \(2019\)](#) fit a model that is cubic in particle velocity,

$$U_s = C_0 + C_1 U_p + C_2 U_p^2 + C_3 U_p^3, \quad (35)$$

which fits into our modeling framework with  $\beta = (C_0, C_1, C_2, C_3)'$  and  $\nu = n - 4$ ; see their Table 4 for estimates of these model parameters for fused silica.

We leave the implementation and further investigation of these points as future work or for interested readers.

## 7 Conclusion

This paper showed how to analyze linear shock compression data in a Bayesian framework. Specifically, under certain standard assumptions, the posterior distribution of the linear model parameters is a bivariate  $t$ -distribution that can be sampled directly. These samples can then be propagated through the Rankine-Hugoniot equations to obtain Hugoniot curves in the pressure-volume plane, or alternatively the posterior distribution can be propagated analytically through the shock wave-particle velocity model to quantify the uncertainty in future shock wave measurements. The method was shown to produce parameter distributions that are less sensitive to the removal of a point with large particle velocity than bootstrapping, though use of either method should also take into account the interpretation of the distributions they produce.

Overall, evaluating the posterior distribution is straightforward and sampling from the distribution is simple, but this perspective on shock compression data also appears to have been overlooked in the literature. For these reasons, this tutorial both fills a gap in the literature and also serves as a useful starting point for practitioners looking to gain familiarity with Bayesian analysis. Additionally, it provides a benchmark for more advanced Bayesian linear model analyses, such as accounting for errors in the particle velocity measurements or relaxing the assumption of independent errors on the shock wave velocity measurements. If either of these more complex models are implemented, their results can be compared against those from the simpler model presented here.

## Acknowledgements

This document was prepared as an account of work sponsored by an agency of the United States government. Neither the United States government nor Lawrence Livermore National Security, LLC, nor any of their employees makes any warranty, expressed or implied, or assumes any legal liability or responsibility for the accuracy, completeness, or usefulness of any information, apparatus, product, or process disclosed, or represents that its use would not infringe privately owned rights. Reference herein to any specific commercial product, process, or service by trade name, trademark, manufacturer, or otherwise does not necessarily constitute or imply its endorsement, recommendation, or favoring by the United States government or Lawrence Livermore National Security, LLC. The views and opinions of authors expressed herein do not necessarily state or reflect those of the United States government or Lawrence Livermore National Security, LLC, and shall not be used for advertising or product endorsement purposes.

Lawrence Livermore National Laboratory is operated by Lawrence Livermore National Security, LLC, for the U.S. Department of Energy, National Nuclear Security Administration under Contract DE-AC52-07NA27344.

**Release Numbers:** LLNL-JRNL-2014240, LA-UR-26-21559

## Author Declarations

### Conflict of Interest

The authors have no conflicts to disclose.

### Author Contributions

**Jason Bernstein:** Conceptualization (equal); Formal analysis (equal); Investigation (equal); Methodology (equal); Software (lead); Visualization (lead); Writing - original draft (lead); Writing - review & editing (equal). **Philip Myint:** Conceptualization (equal); Formal analysis (equal); Investigation (equal); Methodology (equal); Writing - original draft (supporting); Writing - review & editing (equal). **Beth Lindquist:** Conceptualization (equal); Formal analysis (equal); Investigation (equal); Methodology (equal); Writing - original draft (supporting); Writing - review & editing (equal). **Justin Brown:** Conceptualization (equal); Formal analysis (equal); Investigation (equal); Methodology (equal); Writing - original draft (supporting); Writing - review & editing (equal).

## Data Availability

Data sharing is not applicable to this article as no new data were created or analyzed in this study. The data is from [Marsh \(1980\)](#) and can be downloaded from our repository at [github.com/llnl/BALSCD](https://github.com/llnl/BALSCD).

## Appendix A: Overview of Multivariate $t$ -Distribution

A random variable  $X$  is said to have a  $p$ -dimensional  $t$ -distribution with mean  $\mu$ , scale matrix  $\Sigma$ , and  $\nu$  degrees of freedom if it has the probability density function

$$f(x) \propto \left[ 1 + \frac{1}{\nu} (x - \mu)' \Sigma^{-1} (x - \mu) \right]^{-(\nu+p)/2}, \quad (\text{A1})$$

for  $x \in \mathbb{R}^p$ , which is notated

$$X \sim t_p(\mu, \Sigma, \nu). \quad (\text{A2})$$

The proportionality constant is a normalizing constant that ensures  $f(x)$  integrates to one over  $\mathbb{R}^p$ . As  $\nu \rightarrow \infty$ , the distribution converges to a normal distribution with mean  $\mu$  and covariance matrix  $\Sigma$  since

$$\lim_{\nu \rightarrow \infty} f(x) \propto \exp\left(-\frac{1}{2}(x - \mu)' \Sigma^{-1}(x - \mu)\right), \quad (\text{A3})$$

which follows from the exponential function identity

$$\lim_{n \rightarrow \infty} \left(1 + \frac{z}{n}\right)^n = \exp(z) \quad (\text{A4})$$

with  $n = \nu/2$  and  $z$  given by the quadratic form in Eq. (A1) divided by two. When  $\nu = 1$ , the  $t$ -distribution is a Cauchy distribution.

The covariance matrix of  $X$  is  $\nu/(\nu - 2)\Sigma$ . Since the diagonal elements of  $\nu/(\nu - 2)\Sigma$  are greater than the diagonal elements of  $\Sigma$ , the  $t$ -distribution is said to have heavier tails than the normal distribution, though this difference becomes negligible as  $\nu$  increases. Convergence of the univariate  $t$ -distribution to the normal distribution is illustrated in Fig. 10. In practice, the univariate  $t$ -distribution is often approximated as a normal distribution when  $n \geq 30$ .

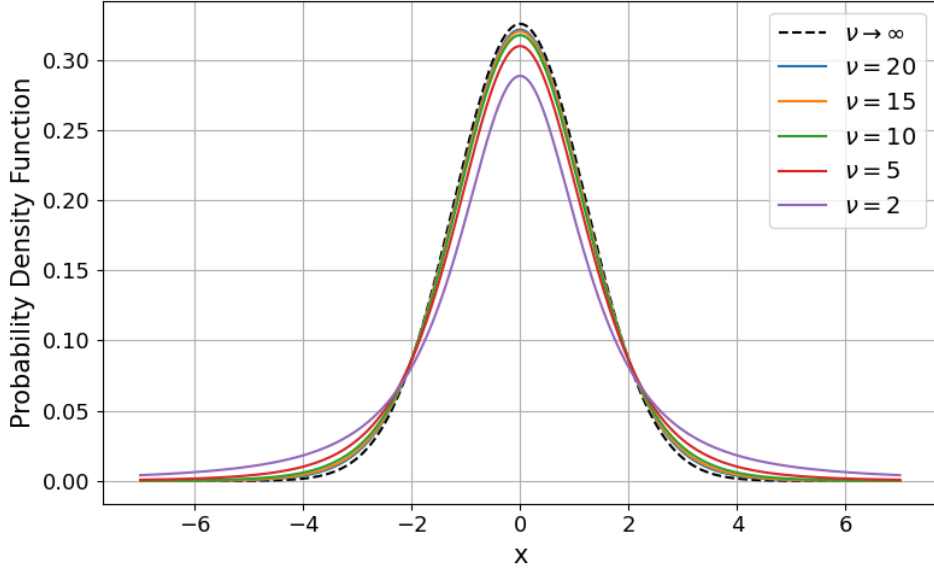


Figure 10: The  $t$ -distribution converges to a normal distribution as the degrees of freedom increases to infinity. For this plot, the dimension of the  $t$ -distribution is  $p = 1$ , the mean is  $\mu = 0$  and the scale matrix is  $\Sigma = 1.5$ , which is a scalar.

## Appendix B: Joint Posterior Distribution of $(\beta, \sigma^2)$

Under the non-informative prior distribution given in Eq. (9), the joint posterior distribution of  $(\beta, \sigma^2)$  is derived as

$$p(\beta, \sigma^2 | Y) \propto p(Y | \beta, \sigma^2) p(\beta, \sigma^2) \quad (\text{B1})$$

$$\propto \frac{1}{(\sigma^2)^{n/2}} \exp\left(-\frac{1}{2\sigma^2} (Y - X\beta)' (Y - X\beta)\right) \frac{1}{\sigma^2} \quad (\text{B2})$$

$$\propto \frac{1}{(\sigma^2)^{n/2}} \exp\left(-\frac{1}{2\sigma^2} (\beta' X' X \beta - 2Y' X \beta + Y' Y)\right) \frac{1}{\sigma^2} \quad (\text{B3})$$

$$\propto \left[ \frac{1}{|\sigma^2 (X' X)^{-1}|^{1/2}} \exp\left(-\frac{1}{2\sigma^2} (\beta - \hat{\beta})' (X' X) (\beta - \hat{\beta})\right) \right] \left[ \frac{1}{(\sigma^2)^{n/2}} \exp\left(-\frac{\nu s^2}{2\sigma^2}\right) \right] \quad (\text{B4})$$

$$\propto p(\beta | \sigma^2, Y) p(\sigma^2 | Y), \quad (\text{B5})$$

where the conditional distribution of  $\beta$  given  $\sigma^2$  and  $Y$  is

$$p(\beta | \sigma^2, Y) \propto \frac{1}{|\sigma^2 (X' X)^{-1}|^{1/2}} \exp\left(-\frac{1}{2\sigma^2} (\beta - \hat{\beta})' (X' X) (\beta - \hat{\beta})\right) \quad (\text{B6})$$

and the marginal posterior distribution of  $\sigma^2$  is

$$p(\sigma^2 | Y) \propto \frac{1}{(\sigma^2)^{n/2}} \exp\left(-\frac{\nu s^2}{2\sigma^2}\right). \quad (\text{B7})$$

The expression in Eq. (B3) is obtained by expanding the quadratic form, and the expression in Eq. (B4) is obtained by completing a matrix square and using the identity

$$s^2 = Y' (I_n - X(X' X)^{-1} X') Y. \quad (\text{B8})$$

The expression in Eq. (B5) implies that  $\beta$ , conditional on  $\sigma^2$  and  $Y$ , has a multivariate normal distribution,

$$\beta | \sigma^2, Y \sim N(\hat{\beta}, \sigma^2 (X' X)^{-1}), \quad (\text{B9})$$

and that the posterior distribution of  $\sigma^2$  is an inverse gamma distribution,

$$\sigma^2 | Y \sim IG\left(\frac{\nu}{2}, \frac{\nu s^2}{2}\right). \quad (\text{B10})$$

As noted in Sec. 3, the joint posterior distribution of  $\beta$  and  $\sigma^2$  is called the normal-inverse-gamma distribution due to this factorization.

## Appendix C: Marginal Posterior Distribution of $\beta$

The marginal posterior distribution of  $\beta$  is obtained by integrating  $\sigma^2$  out of the joint posterior distribution of  $\beta$  and  $\sigma^2$ ,

$$p(\beta | Y) = \int p(\beta, \sigma^2 | Y) d\sigma^2 \quad (\text{C1})$$

$$= \int p(\beta | \sigma^2, Y) p(\sigma^2 | Y) d\sigma^2 \quad (\text{C2})$$

$$\propto \int \frac{1}{(\sigma^2)^{n/2+1}} \exp\left(-\frac{1}{\sigma^2} \left[\frac{1}{2} (\nu s^2 + (\beta - \hat{\beta})' (X' X) (\beta - \hat{\beta}))\right]\right) d\sigma^2 \quad (\text{C3})$$

$$\propto (\nu s^2 + (\beta - \hat{\beta})' (X' X) (\beta - \hat{\beta}))^{-n/2} \quad (\text{C4})$$

$$\propto \left(1 + \frac{1}{\nu} (\beta - \hat{\beta})' \Sigma^{-1} (\beta - \hat{\beta})\right)^{-n/2}. \quad (\text{C5})$$

The last integral is computed using the observation that the integrand is proportional to the probability density function of an inverse gamma distribution with shape parameter  $n/2$  and scale parameter given by the expression in the square brackets. The last expression is the non-normalized density of a  $t_2(\hat{\beta}, \Sigma, \nu)$  distributed random variable, which implies that  $\beta|Y \sim t_2(\hat{\beta}, \Sigma, \nu)$ . Following [Appendix A](#), the marginal posterior mean and covariance matrix of  $\beta$  are  $\hat{\beta}$  and  $\nu/(\nu - 2)\Sigma$ , respectively.

The posterior mean of  $\beta$  can also be computed with the law of total expectation as

$$\mathbb{E}(\beta|Y) = \mathbb{E}(\mathbb{E}(\beta|\sigma^2, Y) | Y) \quad (\text{C6})$$

$$= \mathbb{E}(\hat{\beta}|Y) \quad (\text{C7})$$

$$= \hat{\beta}, \quad (\text{C8})$$

where the second equality follows from [Eq. \(B9\)](#). The posterior covariance matrix of  $\beta$  can be computed with the law of total variance as

$$\text{Var}(\beta|Y) = \mathbb{E}(\text{Var}(\beta|\sigma^2, Y) | Y) + \text{Var}(\mathbb{E}(\beta|\sigma^2, Y) | Y) \quad (\text{C9})$$

$$= \mathbb{E}(\sigma^2(X'X)^{-1}|Y) + \text{Var}(\hat{\beta}|Y) \quad (\text{C10})$$

$$= (X'X)^{-1}\mathbb{E}(\sigma^2|Y) + (X'X)^{-1}X'\text{Var}(Y|Y)X(X'X)^{-1} \quad (\text{C11})$$

$$= (X'X)^{-1} \frac{(n-2)s^2/2}{(n-2)/2-1} \quad (\text{C12})$$

$$= \frac{\nu}{\nu-2}\Sigma. \quad (\text{C13})$$

This derivation uses the fact that  $\sigma^2|Y$  has an inverse gamma distribution given by [Eq. \(12\)](#) and that  $\text{Var}(Y|Y)$  is an  $n \times n$  zero matrix.

## Appendix D: Marginal Posterior Distribution of $\sigma^2$

[Figure 11](#) shows the posterior distributions of the measurement error variance parameter,  $\sigma^2$ , for the three datasets shown in [Fig. 2](#). Recall from [Eq. \(12\)](#) that these are inverse gamma distributions with shape and scale parameters given by  $a = (n-2)/2$  and  $b = (n-2)s^2/2$ , respectively. The posterior mean of  $\sigma^2$  is

$$\mathbb{E}(\sigma^2|Y) = \frac{b}{a-1}, \quad (\text{D1})$$

which is defined for  $n > 4$ , and the posterior variance of  $\sigma^2$  is

$$\text{Var}(\sigma^2|Y) = \frac{b^2}{(a-1)^2(a-2)}, \quad (\text{D2})$$

which is defined for  $n > 6$ . The posterior mean and standard deviation are both shown in the upper right corner of the plots. Note that the distributions are right skewed and that of these three datasets, the posterior mean and variance of  $\sigma^2$  is greatest for argon. This makes sense given that the residuals for argon appear to have greater spread, on average, than the residuals for copper or nickel, as shown in [Fig. 12](#). The skew does decrease as the number of measurements increases, with the distribution for copper appearing almost normal.

## Appendix E: Posterior Predictive Distribution

The posterior predictive distribution for a new shock wave velocity measurement,  $p(\tilde{y}|Y)$ , given in [Eq. \(31\)](#), can be derived as follow. The future measurement,  $\tilde{Y}$ , is modeled as

$$\tilde{Y} = \mathbf{x}'_*\beta + \tilde{\epsilon}, \quad (\text{E1})$$

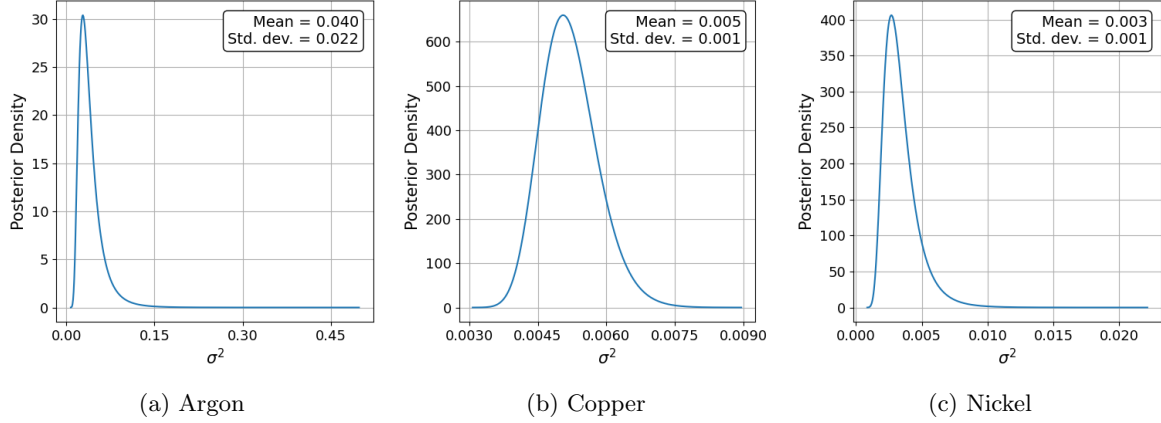


Figure 11: Marginal posterior distributions of the variance of the measurement error, or  $p(\sigma^2|Y)$ .

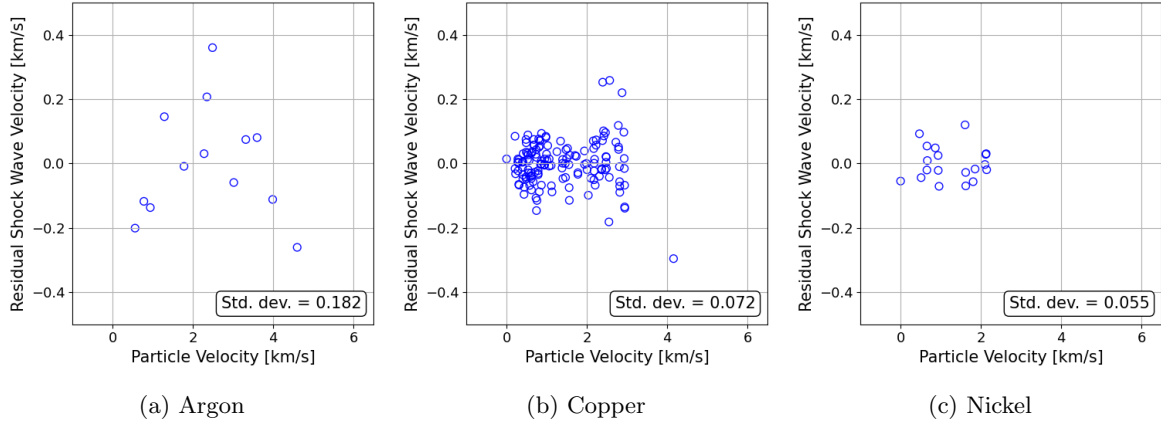


Figure 12: Residual shock wave velocities from the least squares fits. The standard deviation of the residuals is the square root of the sample variance,  $s^2$ .

where  $\tilde{\epsilon} \sim N(0, \sigma^2)$ . Since

$$\beta|\sigma^2, Y \sim N(\hat{\beta}, \sigma^2(X'X)^{-1}) \quad (\text{E2})$$

from Eq. (11), it follows from multiplying through by  $\mathbf{x}'_*$  and adding  $\tilde{\epsilon}$  that

$$\tilde{Y}|\sigma^2, Y \sim N(\mathbf{x}'_*\hat{\beta}, \sigma^2(1 + \mathbf{x}'_*(X'X)^{-1}\mathbf{x}_*)). \quad (\text{E3})$$

The posterior predictive distribution is obtained by integrating  $\sigma^2$  out of the distribution in Eq. (E3). That is,

$$p(\tilde{y}|Y) = \int p(\tilde{y}|\sigma^2, Y)p(\sigma^2|Y) d\sigma^2 \quad (\text{E4})$$

$$\propto \int \frac{1}{(\sigma^2)^{1/2}} \exp\left(-\frac{(\tilde{y} - \mathbf{x}'_*\hat{\beta})^2}{2\sigma^2(1 + \mathbf{x}'_*(X'X)^{-1}\mathbf{x}_*)}\right) \frac{1}{(\sigma^2)^{n/2}} \exp\left(-\frac{\nu s^2}{2\sigma^2}\right) d\sigma^2 \quad (\text{E5})$$

$$\propto \int \frac{1}{(\sigma^2)^{(n+1)/2}} \exp\left(-\frac{1}{\sigma^2} \left[ \frac{(\tilde{y} - \mathbf{x}'_*\hat{\beta})^2}{2(1 + \mathbf{x}'_*(X'X)^{-1}\mathbf{x}_*)} + \frac{\nu s^2}{2} \right]\right) d\sigma^2 \quad (\text{E6})$$

$$\propto \left[ 1 + \frac{(\tilde{y} - \mathbf{x}'_*\hat{\beta})^2}{\nu s^2(1 + \mathbf{x}'_*(X'X)^{-1}\mathbf{x}_*)} \right]^{-(n-1)/2}, \quad (\text{E7})$$

where  $p(\sigma^2|Y)$  is given in Eq. (B7). The last integral is computed using the observation that the integrand is the non-normalized density of an inverse gamma distributed random variable with shape parameter  $\tilde{a} = (n - 1)/2$  and scale parameter, say  $\tilde{b}$ , given by the expression in the square brackets. Since the integral of a probability density function over its support equals one, the last integral is proportional to  $\tilde{b}^{-\tilde{a}}$ . The last expression is the non-normalized density of a univariate  $t$ -distribution with  $\nu$  degrees of freedom, mean  $\mathbf{x}'_*\hat{\beta}$ , and scale matrix  $s^2(1 + \mathbf{x}'_*(X'X)^{-1}\mathbf{x}_*)$ , which implies that the posterior predictive distribution is as given in Eq. (32).

## Appendix F: Credible Intervals for $C_0$ and $S$

To derive the credible interval for  $C_0$  given in Eq. (21), first note that if the scale matrix  $\Sigma$  is written as

$$\Sigma = \begin{pmatrix} \sigma_{11}^2 & \rho\sigma_{11}\sigma_{22} \\ \rho\sigma_{11}\sigma_{22} & \sigma_{22}^2 \end{pmatrix}, \quad (\text{F1})$$

where  $\rho \in (-1, 1)$  is a correlation parameter, then the Cholesky decomposition of the scale matrix is

$$L = \begin{pmatrix} \sigma_{11} & 0 \\ \rho\sigma_{22} & \sigma_{22}\sqrt{1-\rho^2} \end{pmatrix}. \quad (\text{F2})$$

Hence, multiplying Eq. (26) through by the vector  $(1, 0)$  yields

$$C_0 = \sigma_{11}Z_1\sqrt{\nu/W} + \hat{C}_0, \quad (\text{F3})$$

which implies that  $(C_0 - \hat{C}_0)/\sigma_{11}$  has a univariate  $t$ -distribution with  $\nu$  degrees of freedom. It follows that

$$p\left(t_{0.025,\nu} < \frac{C_0 - \hat{C}_0}{\sigma_{11}} < t_{0.975,\nu}\right) = 0.95, \quad (\text{F4})$$

where  $t_{0.025,\nu}$  and  $t_{0.975,\nu}$  are the 0.025th and 0.975th quantiles of a univariate  $t$ -distribution with  $\nu$  degrees of freedom, respectively. Equivalently,

$$p(\hat{C}_0 + t_{0.025,\nu}\sigma_{11} < C_0 < \hat{C}_0 + t_{0.975,\nu}\sigma_{11}) = 0.95, \quad (\text{F5})$$

which proves that the credible interval for  $C_0$  is given by Eq. (21). The credible interval for  $S$  given by Eq. (22) is derived similarly by multiplying Eq. (26) through by the vector  $(0, 1)$  instead of  $(1, 0)$ .

## Appendix G: Credible Region for $\beta$

Recall from Sec. 3 that a credible region for  $\beta$  is a set of possible values of  $\beta$ , denoted  $\mathcal{R}_\alpha$ , such that  $p(\beta \in \mathcal{R}_\alpha|Y) = 1 - \alpha$  for some  $\alpha \in (0, 1)$ . To derive a credible region for  $\beta$ , it follows from Eq. (26) that

$$L^{-1/2}(\beta - \hat{\beta}) = \frac{Z}{\sqrt{W/\nu}}, \quad (\text{G1})$$

or equivalently

$$\frac{(\beta - \hat{\beta})'\Sigma^{-1}(\beta - \hat{\beta})}{2} = \frac{Z'Z/2}{W/\nu}. \quad (\text{G2})$$

The right side of the last expression is the ratio of two independent chi-square random variables divided by their degrees of freedom, and therefore it has an  $F$ -distribution with 2 and  $\nu$  degrees of freedom, denoted  $F_{2,\nu}$ . Hence, a credible region is

$$\mathcal{R}_\alpha = \{\beta | (\beta - \hat{\beta})'\Sigma^{-1}(\beta - \hat{\beta}) \leq 2F_{1-\alpha,2,\nu}\}, \quad (\text{G3})$$

where  $F_{1-\alpha,2,\nu}$  is the  $(1-\alpha)$ th quantile of an  $F_{2,\nu}$  distribution. The credible region is an ellipse whose semi-major axes have lengths  $\sqrt{2\lambda_i F_{1-\alpha,2,\nu}}$  for  $i = 1$  and  $2$ , where  $\lambda_1$  and  $\lambda_2$  are the eigenvalues of  $\Sigma$ . To derive the semi-major axes, first diagonalize the scale matrix of the posterior distribution as

$$\Sigma = U\Lambda U', \quad (\text{G4})$$

where  $U$  is a matrix whose columns are the eigenvectors of  $\Sigma$  and  $\Lambda$  is a diagonal matrix whose diagonal elements are  $\lambda_1$  and  $\lambda_2$ , and define  $\eta = (\eta_1, \eta_2)'$  as

$$\eta = U'(\beta - \hat{\beta}). \quad (\text{G5})$$

Plugging this expression for  $\Sigma$  into the credible region and simplifying the resulting expression yields

$$\mathcal{R}_\alpha = \left\{ \begin{pmatrix} \eta_1 \\ \eta_2 \end{pmatrix} \mid \frac{\eta_1^2}{2F_{1-\alpha,2,\nu}\lambda_1} + \frac{\eta_2^2}{2F_{1-\alpha,2,\nu}\lambda_2} \leq 1 \right\}, \quad (\text{G6})$$

which is an ellipse with the claimed semi-major axes. The red ellipses in Fig. 4 are boundaries of 95% credible regions with  $\alpha = 0.05$ .

## Appendix H: Informative Prior Distribution

In some cases, there is prior information about  $\beta$  and  $\sigma^2$  that can be used to construct a prior distribution. A normal-inverse-gamma distribution is a common choice of prior distribution in this situation because it leads to a normal-inverse-gamma posterior distribution, a property referred to as conjugacy. This prior is written as

$$p(\beta, \sigma^2) = p(\beta|\sigma^2)p(\sigma^2), \quad (\text{H1})$$

where  $\beta|\sigma^2$  is a normal distribution with mean  $\beta_0$  and covariance matrix  $\sigma^2\Sigma_0$ , and where  $\sigma^2$  has an inverse gamma distribution with shape parameter  $a_0$  and scale parameter  $b_0$ . The prior mean for  $\beta$  is then

$$\mathbf{E}(\beta) = \mathbf{E}(\mathbf{E}(\beta|\sigma^2)) \quad (\text{H2})$$

$$= \mathbf{E}(\beta_0) \quad (\text{H3})$$

$$= \beta_0, \quad (\text{H4})$$

and the prior covariance matrix is

$$\text{Var}(\beta) = \text{Var}(\mathbf{E}(\beta|\sigma^2)) + \mathbf{E}(\text{Var}(\beta|\sigma^2)) \quad (\text{H5})$$

$$= \text{Var}(\beta_0) + \mathbf{E}(\sigma^2\Sigma_0) \quad (\text{H6})$$

$$= \frac{b_0}{a_0 - 1}\Sigma_0, \quad (\text{H7})$$

since the elements of the covariance matrix of  $\beta_0$  are all zeros. Hence, the prior mean and covariance information about  $\beta$  can be summarized by choosing  $\beta_0$ ,  $\Sigma_0$ ,  $a_0$ , and  $b_0$ . For example, decreasing the diagonal elements of  $\Sigma_0$  shrinks the prior uncertainty in  $\beta$ . This prior distribution is said to be informative since it biases the posterior distribution towards particular values of  $\beta$  and  $\sigma^2$ . The prior mean and covariance matrix could also be obtained by noting that the marginal prior distribution for  $\beta$  is a  $t$ -distribution,

$$\beta \sim t_2 \left( \beta_0, \frac{b_0}{a_0}\Sigma_0, 2a_0 \right), \quad (\text{H8})$$

though we omit this derivation since it is similar to others given in this tutorial where  $\sigma^2$  is integrated out of the joint prior distribution of  $\beta$  and  $\sigma^2$ .

Under this prior distribution, the joint posterior distribution of  $\beta$  and  $\sigma^2$  is the product of posterior distributions for  $\beta$  and  $\sigma^2$ ,

$$p(\beta, \sigma^2|Y) \propto p(\beta|\sigma^2, Y)p(\sigma^2|Y). \quad (\text{H9})$$

The posterior distribution of  $\beta$ , conditional on  $\sigma^2$ , is a normal distribution,

$$\beta|\sigma^2, Y \sim N(\tilde{\beta}, \sigma^2 G^{-1}), \quad (\text{H10})$$

where

$$G = X'X + \Sigma_0^{-1} \quad (\text{H11})$$

$$\gamma = X'Y + \Sigma_0^{-1}\beta_0 \quad (\text{H12})$$

$$= X'X\hat{\beta} + \Sigma_0^{-1}\beta_0, \quad (\text{H13})$$

and

$$\tilde{\beta} = G^{-1}\gamma. \quad (\text{H14})$$

Note that the posterior mean,  $\tilde{\beta}$ , is a weighted average of the least squares estimate,  $\hat{\beta}$ , and the prior mean  $\beta_0$ . The marginal posterior distribution of  $\sigma^2$  is an inverse gamma distribution,

$$\sigma^2|Y \sim IG(\tilde{a}, \tilde{b}), \quad (\text{H15})$$

where the shape parameter is

$$\tilde{a} = a_0 + \frac{n}{2} \quad (\text{H16})$$

and the scale parameter is

$$\tilde{b} = b_0 + \frac{1}{2}[Y'Y + \beta_0'\Sigma_0^{-1}\beta_0 - \gamma'G^{-1}\gamma]. \quad (\text{H17})$$

The derivation of this result is standard,

$$p(\beta, \sigma^2|Y) \propto p(Y|\beta, \sigma^2)p(\beta|\sigma^2)p(\sigma^2) \quad (\text{H18})$$

$$\propto \frac{1}{(\sigma^2)^{n/2}} \exp\left(-\frac{1}{2\sigma^2}(Y - X\beta)'(Y - X\beta)\right) \frac{1}{\sigma^2} \exp\left(-\frac{1}{2\sigma^2}(\beta - \beta_0)'\Sigma_0^{-1}(\beta - \beta_0)\right) \quad (\text{H19})$$

$$\frac{1}{(\sigma^2)^{a_0+1}} \exp\left(-\frac{b_0}{\sigma^2}\right) \quad (\text{H20})$$

$$\propto \frac{1}{\sigma^2} \exp\left(-\frac{1}{2\sigma^2}[\beta'X'X\beta - 2\beta'X'Y + \beta'\Sigma_0^{-1}\beta - 2\beta'\Sigma_0^{-1}\beta_0]\right) \quad (\text{H21})$$

$$\frac{1}{(\sigma^2)^{\tilde{a}+1}} \exp\left(-\frac{1}{\sigma^2}[b_0 + \frac{1}{2}(Y'Y + \beta_0'\Sigma_0^{-1}\beta_0)]\right) \quad (\text{H22})$$

$$\propto \frac{1}{\sigma^2} \exp\left(-\frac{1}{2\sigma^2}[\beta'G\beta - 2\beta'\gamma]\right) \frac{1}{(\sigma^2)^{\tilde{a}+1}} \exp\left(-\frac{1}{\sigma^2}[b_0 + \frac{1}{2}(Y'Y + \beta_0'\Sigma_0^{-1}\beta_0)]\right) \quad (\text{H23})$$

$$\propto \left[\frac{1}{\sigma^2} \exp\left(-\frac{1}{2\sigma^2}(\beta - \tilde{\beta})'G(\beta - \tilde{\beta})\right)\right] \left[\frac{1}{(\sigma^2)^{\tilde{a}+1}} \exp\left(-\frac{\tilde{b}}{\sigma^2}\right)\right]. \quad (\text{H24})$$

Note that this posterior distribution is the product of a normal distribution for  $\beta$  and an inverse gamma distribution for  $\sigma^2$ , and is an example of the normal-inverse-gamma distribution mentioned earlier.

The marginal posterior distribution of  $\beta$  under the informative prior is derived as

$$p(\beta|Y) \propto \int p(\beta, \sigma^2|Y) d\sigma^2 \quad (\text{H25})$$

$$\propto \int \frac{1}{(\sigma^2)^{\tilde{a}+2}} \exp\left(-\frac{1}{\sigma^2} \left[\tilde{b} + \frac{(\beta - \tilde{\beta})'G(\beta - \tilde{\beta})}{2}\right]\right) d\sigma^2 \quad (\text{H26})$$

$$\propto \left[\tilde{b} + \frac{(\beta - \tilde{\beta})'G(\beta - \tilde{\beta})}{2}\right]^{-(2\tilde{a}+2)/2} \quad (\text{H27})$$

$$\propto \left[1 + \frac{(\beta - \tilde{\beta})'G(\beta - \tilde{\beta})}{2\tilde{b}}\right]^{-(2\tilde{a}+2)/2} \quad (\text{H28})$$

$$\propto \left[1 + \frac{(\beta - \tilde{\beta})'[\frac{\tilde{b}}{\tilde{a}}G^{-1}]^{-1}(\beta - \tilde{\beta})}{2\tilde{a}}\right]^{-(2\tilde{a}+2)/2}, \quad (\text{H29})$$

where the integral is obtained using the fact that the probability density function of the inverse gamma distribution integrates to one. This implies that the marginal distribution of  $\beta$  is a bivariate  $t$ -distribution with mean  $\tilde{b}$ , scale matrix  $(\tilde{b}/\tilde{a})G^{-1}$ , and  $2\tilde{a}$  degrees of freedom, or

$$\beta|Y \sim t_2\left(\tilde{\beta}, \frac{\tilde{b}}{\tilde{a}}G^{-1}, 2\tilde{a}\right). \quad (\text{H30})$$

The marginal posterior distribution of  $\beta$  under the non-informative prior derived in [Appendix C](#) is obtained as  $a_0 \rightarrow 0$ ,  $b_0 \rightarrow 0$ , and as the elements of  $\Sigma_0^{-1}$  converge to zero. Samples from this distribution can be obtained as described in [Sec. 4](#).

[Figure 13](#) shows the marginal posterior distributions of  $\beta$  assuming an informative prior distribution. Note that the least squares estimates, the blue dots, are the posterior means under the non-informative prior distributions. Hence, we see that the informative prior distributions pull the posterior mean away from the least squares estimates. Note as well that although the prior distributions are informative, the variances are still large. In this situation, the prior distributions are referred to as weakly informative. To generate this plot, we set the prior correlation for argon, copper, and nickel to be 0, -0.2, and -0.8, respectively. This explains why the prior distributions are increasingly slanted for argon, copper, and nickel.

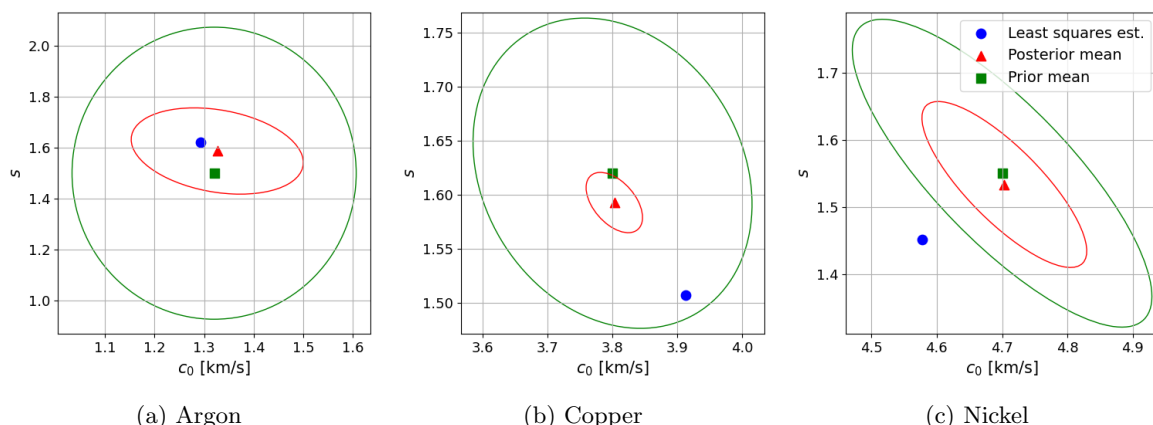


Figure 13: Posterior  $t$ -distributions for  $\beta = (C_0, S)'$  under informative prior distributions. The green ellipses are 95% probability regions for the prior mean,  $\beta_0$ , and the red ellipses are 95% credible regions for the posterior mean,  $\hat{\beta}$ . Each posterior mean,  $\hat{\beta}$ , is a weighted average of the least squares estimate and the prior mean.

## Appendix I: Bootstrap Confidence and Prediction Intervals for Shock Wave Velocity

Figure 14 shows bootstrap confidence intervals for the mean shock wave velocity and prediction intervals for new shock wave velocity measurements. The plot is created by first resampling the original data 100,000 times to create a large collection of bootstrap datasets. For each bootstrap dataset, we compute  $\hat{\beta}$  and then evaluate the corresponding shock wave across a grid of particle velocities. This results in 100,000 shock wave-particle velocity curves, whose mean is called the bootstrap mean in the figure. The 95% confidence intervals are computed as the 2.5th and 97.5th percentiles of this ensemble of shock wave-particle velocity curves. The prediction intervals are obtained by adding normally distributed random variables with variance  $s^2$  to the simulated shock wave velocity data, and then taking the 2.5th and 97.5th percentiles of the curves. Overall, the means and intervals in Fig. 14 appear close to those in Fig. 6, which shows credible and prediction intervals for the posterior distribution.

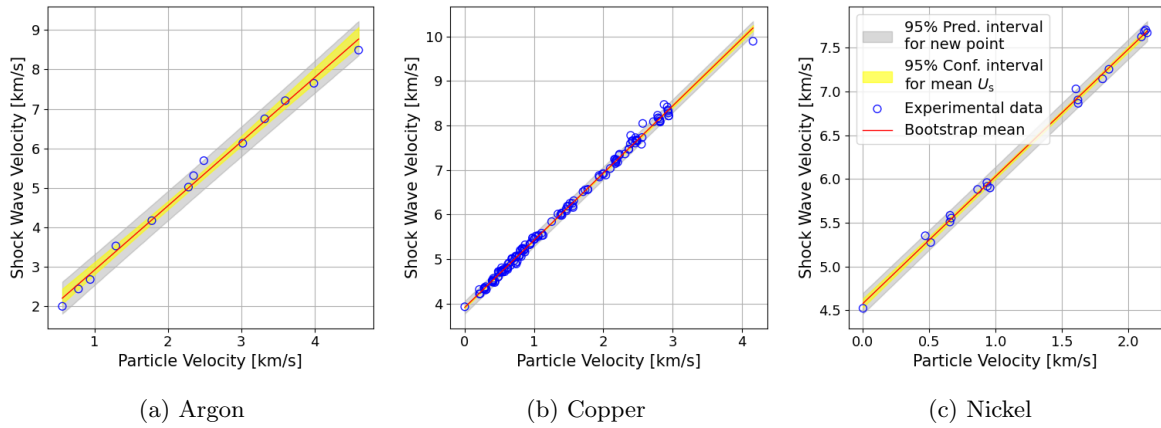


Figure 14: Bootstrap confidence intervals for the mean shock wave velocity and prediction intervals for new shock wave velocity measurements.

## Appendix J: Convergence of $t$ -Distribution to Normal Distribution

Recall from Eq. (26) that if  $W \sim \chi_\nu^2$  and  $Z \sim N(0, I)$ , then  $LZ\sqrt{\nu/W} + \mu$  is a multivariate  $t$ -distribution with mean  $\mu$  and covariance matrix  $\Sigma = LL'$ . Now,  $W/\nu \rightarrow 1$  in probability as  $\nu \rightarrow \infty$  by the weak law of large numbers (Resnick, 2019, Theorem 7.2.1), which implies that  $\sqrt{W}/\nu \rightarrow 1$  in probability as  $\nu \rightarrow \infty$  by the continuous mapping theorem (Resnick, 2019, Corollary 8.3.1). Since  $Z \rightarrow Z$  in distribution as  $\nu \rightarrow \infty$ , it follows from Slutsky's Theorem (Resnick, 2019, Theorem 8.6.1) that  $Z\sqrt{\nu/W}$  converges in distribution to a  $N(0, I)$  distribution as  $\nu \rightarrow \infty$ , and so  $LZ\sqrt{\nu/W} + \mu$  converges to a  $N(\mu, \Sigma)$  distribution.

## References

- Ahrens, T. J. (1993). Equation of state. In *High-Pressure Shock Compression of Solids*, pages 75–113. Springer.
- Ali, S., Swift, D., Wu, C., and Kraus, R. (2020). Development of uncertainty-aware equation-of-state models: Application to copper. *Journal of Applied Physics*, 128(18).
- Banerjee, S. (2008). Bayesian linear model: Gory details. <https://ams206-winter19-01.courses.soe.ucsc.edu/system/files/attachments/banerjee-bayesian-linear-model-details.pdf>.
- Brown, J. L., Davis, J.-P., Tucker, J. D., Huerta, G., and Shuler, K. W. (2023). Quantifying uncertainty in analysis of shockless dynamic compression experiments on platinum. II. Bayesian model calibration. *Journal of Applied Physics*, 134(23).
- Brynjarsdóttir, J. and O’Hagan, A. (2014). Learning about physical parameters: The importance of model discrepancy. *Inverse Problems*, 30(11):114007.
- Carroll, R. J., Ruppert, D., Stefanski, L. A., and Crainiceanu, C. M. (2006). *Measurement error in nonlinear models: A modern perspective*. Chapman and Hall/CRC.
- Celliers, P., Collins, G., Hicks, D., and Eggert, J. (2005). Systematic uncertainties in shock-wave impedance-match analysis and the high-pressure equation of state of Al. *Journal of Applied Physics*, 98(11).
- Chib, S. (2001). Markov chain monte carlo methods: Computation and inference. *Handbook of Econometrics*, 5:3569–3649.
- DiCiccio, T. J. and Efron, B. (1996). Bootstrap confidence intervals. *Statistical science*, 11(3):189–228.
- Duvall, G. and Graham, R. (1977). Phase transitions under shock-wave loading. *Reviews of Modern Physics*, 49(3):523.
- Forbes, J. W. (2012). *Shock wave compression of condensed matter: A primer*. Springer.
- Foreman-Mackey, D., Hogg, D. W., Lang, D., and Goodman, J. (2013). emcee: the MCMC hammer. *Publications of the Astronomical Society of the Pacific*, 125(925):306.
- Gelman, A., Carlin, J. B., Stern, H. S., and Rubin, D. B. (1995). *Bayesian data analysis*. Chapman and Hall/CRC.
- Gelman, A., Vehtari, A., Simpson, D., Margossian, C. C., Carpenter, B., Yao, Y., Kennedy, L., Gabry, J., Bürkner, P.-C., and Modrák, M. (2020). Bayesian workflow. *arXiv preprint arXiv:2011.01808*.
- Hesterberg, T. (2011). Bootstrap. *Wiley Interdisciplinary Reviews: Computational Statistics*, 3(6):497–526.
- Hofert, M. (2013). On sampling from the multivariate t distribution. *The R Journal*, 5(2):129–136.
- Huijser, D., Goodman, J., and Brewer, B. J. (2022). Properties of the affine-invariant ensemble sampler’s ‘stretch move’ in high dimensions. *Australian & New Zealand Journal of Statistics*, 64(1):1–26.
- Levashov, P. R., Khishchenko, K. V., Lomonosov, I. V., and Fortov, V. E. (2004). Database on shock-wave experiments and equations of state available via internet. In *AIP Conference Proceedings*, volume 706, pages 87–90. American Institute of Physics.
- Lindquist, B. A., Jadrach, R. B., Heras Rivera, J. E., and Rondini, L. I. (2023). Uncertainty quantification for high explosive reactant and product equations of state. *Journal of Applied Physics*, 134(7).
- Lindquist, B. A., Rudin, S. P., and Rehn, D. A. (2024). Uncertainty quantification for equation of state using heterogeneous data sources. In *AIP Conference Proceedings*, volume 3066, page 470004. AIP Publishing LLC.

- Marsh, S. P. (1980). *LASL shock Hugoniot data*, volume 5. University of California Press.
- More, R. M., Warren, K. H., Young, D. A., and Zimmerman, G. B. (1988). A new quotidian equation of state (QEOS) for hot dense matter. *Phys. Fluids*, 31:3059–3078.
- Myint, P. C., Root, S., Wu, C. J., Clay, R. C., Lopez, A., Hanshaw, H. L., Lemke, R. W., Bliss, D. E., Hanson, D. L., Flicker, D. G., and Long, Z. C. (2023). Fluid-phase helium: Shock-compression experiments, quantum molecular dynamics simulations, and development of an equation of state. *Phys. Rev. B*, 108:134202.
- Nellis, W. (1990). Shock compression of solids: A tutorial. Technical report, Lawrence Livermore National Lab. (LLNL), Livermore, CA (United States).
- Rencher, A. C. and Schaalje, G. B. (2008). *Linear models in statistics*. John Wiley & Sons.
- Resnick, S. (2019). *A probability path*. Springer.
- Robinson, A. C., Berry, R., Carpenter, J., Debusschere, B., Drake, R. R., Mattsson, A., and Rider, W. J. (2013). Fundamental issues in the representation and propagation of uncertain equation of state information in shock hydrodynamics. *Computers & Fluids*, 83:187–193.
- Root, S., Townsend, J. P., and Knudson, M. D. (2019). Shock compression of fused silica: An impedance matching standard. *Journal of Applied Physics*, 126(16).
- Rubin, D. B. (1981). The bayesian bootstrap. *The annals of statistics*, pages 130–134.
- Wu, C. J., Myint, P. C., Pask, J. E., Prisbrey, C. J., Correa, A. A., Suryanarayana, P., and Varley, J. B. (2021). Development of a multiphase beryllium equation of state and physics-based variations. *J. Phys. Chem. A*, 125:1610–1636.